研究成果の刊行に関する一覧表

研究分担者　国立感染症研究所エイズ研究センター　村上　努

雑誌

発表者氏名	論文タイトル名	発表誌名	巻号	ページ	出版年
Narumi T, Aikawa H, Tanaka T, Hashimoto C, Ohashi N, Nomura W, Kobayakawa T, Takano H, Hirota Y, Murakami T, Yamamoto N, Tamamura H	Low-molecular-weight CXCR4 ligands with variable spacers.	Chem Med Chem	8(1)	118-124	2012
Takemura T, Murakami T	Functional constraints on HIV-1 capsid: their impacts on the viral immune escape potency.	Front Microbiol	3	369	2012
Miyauchi K, Urano E, Takeda S, Murakami T, Okada Y, Cheng K, Yin H, Kubo M, Komano J	Toll-like receptor (TLR) 3 as a surrogate sensor of retroviral infection in human cells.	Biochem Biophys Res Commun	424 (3)	519-523	2012
Nakasone T, Kumakura S, Yamamoto M, Murakami T, Yamamoto N	Single oral administration of the novel CXCR4 antagonist, KRH-3955, induces an efficient and long-lasting increase of white blood cell count in normal macaques, and prevents CD4 depletion in SHIV-infected macaques.	Med Microbiol Immunol	202 (2)	175-182	2012
Nakasone T, Murakami T, Yamamoto N	Double oral administrations of emtricitabine/tenofovir prior to virus exposure protects against highly pathogenic SHIV infection in macaques.	Jpn J Infect Dis	65	345-349	2012
Narumi T, Tanaka T, Hashimoto C, Nomura W, Aikawa W, Sohma A, Itotani K, Kawamata M, Murakami T, Yamamoto N, Tamamura H	Pharmacophore-based small molecule CXCR4 ligands.	Biorg Med Chem Lett	22	4169-4172	2012
Yanagita H, Fudo S, Urano E, Ichikawa R, Ogata M, Yokota Y, Murakami T, Wu H, Chiba J, Komano J, Hoshino T:	Structural modulation study of inhibitory compounds for RNase H activity of HIV-1 reverse transcriptase.	Chem Pharm Bull	60	764-771	2012
竹村太地郎、村上　努	宿主とのインターフェイスとしての HIV-1 キャプシドタンパク質の役割	J. AIDS Res	14(2)	10-15	2012

村上　努、高橋秀実	HIV と闘う宿主防御因子序論	J. AIDS Res	14(1)	1-2	2012
M. A. Checkley, B. G. Luttge, P. Y. Mercredi, S. K. Kyere, J. Donlan, Murakami T, M. F. Summers, S. Cocklin, E. O. Freed	Reevaluation of the requirement for TIP47 in human immunodeficiency virus type 1 envelope glycoprotein incorporation.	J Virol	87(6)	3561-3570	2013
Takemura T, Kawamata M, Urabe M, Murakami T	Cyclophilin A-dependent restriction to capsid N121K mutant human immunodeficiency virus type 1 in a broad range of cell lines.	J Virol	87(7)	4086-4090	2013

Bioorganic & Medicinal Chemistry Letters 22 (2012) 4169–4172

Contents lists available at SciVerse ScienceDirect

Bioorganic & Medicinal Chemistry Letters

journal homepage: www.elsevier.com/locate/bmcl

Pharmacophore-based small molecule CXCR4 ligands

Tetsuo Narumi [a], Tomohiro Tanaka [a], Chie Hashimoto [a], Wataru Nomura [a], Haruo Aikawa [a], Akira Sohma [a], Kyoko Itotani [a], Miyako Kawamata [b], Tsutomu Murakami [b], Naoki Yamamoto [c], Hirokazu Tamamura [a,*]

[a] Institute of Biomaterials and Bioengineering, Tokyo Medical and Dental University, Chiyoda-ku, Tokyo 101-0062, Japan
[b] AIDS Research Center, National Institute of Infectious Diseases, Shinjuku-ku, Tokyo 162-8640, Japan
[c] Yong Loo Lin School of Medicine, National University of Singapore, Singapore 117597, Singapore

ARTICLE INFO

Article history:
Received 16 March 2012
Revised 4 April 2012
Accepted 7 April 2012
Available online 20 April 2012

Keywords:
HIV entry inhibitors
Chemokine receptor
AIDS
Low molecular weight CXCR4 ligands

ABSTRACT

Low molecular weight CXCR4 ligands were developed based on the peptide T140, which has previously been identified as a potent CXCR4 antagonist. Some compounds with naphthyl, fluorobenzyl and pyridyl moieties as pharmacophore groups in the molecule showed significant CXCR4-binding activity and anti-HIV activity. Structure–activity relationships were studied and characteristics of each of these three moieties necessary for CXCR4 binding were defined. In this way, CXCR4 ligands with two types of recognition modes for CXCR4 have been found.

The chemokine receptor CXCR4 is classified into a family of G protein-coupled receptors (GPCRs), and transduces signals of its endogenous ligand, CXCL12/stromal cell-derived factor-1 (SDF-1).[1] The CXCR4-CXCL12 axis plays a physiological role in chemotaxis,[2] angiogenesis[3] and neurogenesis[4] in embryonic stages. The CXCR4 receptor is linked to many disorders including HIV infection/AIDS,[5] metastasis of cancer cells,[6] leukemia cell progression,[7] rheumatoid arthritis.[8] Since CXCR4 is an important drug target in these diseases, it is thought that effective agents directed to this receptor may be useful leads for therapeutic agents. To date, we and others have developed several potent CXCR4 antagonists. A highly potent antagonist, T140, a 14-mer peptide with a disulfide bridge, and its downsized analogue, FC131, with a cyclic pentapeptide scaffold, and several other related compounds have been reported.[9] Based on T140 and FC131, small-sized linear anti-HIV agents such as ST34 (**1**) have been developed (Fig. 1).[10] AMD3100,[11] KRH-1636,[12] Dpa–Zn complex (**2**)[13] and other azamacrocyclic compounds such as **3**,[14] which like **1**, contain benzylamine and electron-deficient aromatic groups, have also been reported as nonpeptidic antagonists. Compound **1** possesses significant anti-HIV activity but does not have high CXCR4 binding affinity. In the present study, more effective linear CXCR4 antagonists derived from compound **1** have been examined, and structure–activity relationship studies of these compounds have been performed.

Initially, three segments of compound **1** were selected for structural modification to support the design of new synthetic compounds: replacement of the 4-trifluoromethylbenzoyl group (Fig. 2, R^1), modification of the stereochemistry of the 1-naphthylethylamine moiety (R^2) and introduction of pyridine moieties on the nitrogen atom (R^3). In a previous study of T140 analogues, 4-fluorobenzoyl was found to be superior to 4-trifluoromethylbenzoyl as an N-terminal moiety. Thus, 4-fluorobenzyl, 4-fluorobenzoyl and 4-fluorophenylethyl groups were used as substitutes for the 4-trifluoromethylbenzoyl group (R^1) in **1**. The (*R*)-1-naphthylethylamine moiety in **1** is also present in KRH-1636 where it has the (*S*)-stereochemistry and thus both the (*R*) and (*S*)-stereoisomers were investigated in the present study. Several CXCR4 antagonists such as KRH-1636,[12] Dpa-Zn complex (**2**)[13] and Dpa-cyclam compound (**3**),[14] contain pyridyl rings. Thus, 2, 3, or 4-pyridylmethyl and 2, 3, or 4-pyridylethyl groups were introduced on the nitrogen atom of the 4-aminomethylbenzoyl group (R^3). With these modifications, a total of $3 \times 2 \times 6 = 36$ compounds (**12–47**) were designed (Fig. 2).

The synthesis of the structural fragment, Unit 1 is shown in Scheme 1. N-nosylation of 4-amino-methylbenzoic acid (**4**) with 2-nitrobenzenesulfonyl chloride and subsequent esterification gave the *t*-butyl ester **5**. Introduction of an R^3 moiety by means of a Mitsunobu reaction followed by removal of the Ns group yielded amines **6A–F**. Introduction of either 4-fluorobenzyl or 4-fluorophenylethyl groups by reductive amination of **6A–F** produced amines **7Ai–Fi** or **7Aiii–Fiii**, respectively. Conversion of **6A–F** to the appropriate amide (**7Aii-Fii**), and subsequent deprotection of the *tert*-butyl group yielded Unit 1, **8Ai–Fiii**.

* Corresponding author.
E-mail address: tamamura.mr@tmd.ac.jp (H. Tamamura).

0960-894X/$ - see front matter © 2012 Elsevier Ltd. All rights reserved.
http://dx.doi.org/10.1016/j.bmcl.2012.04.032

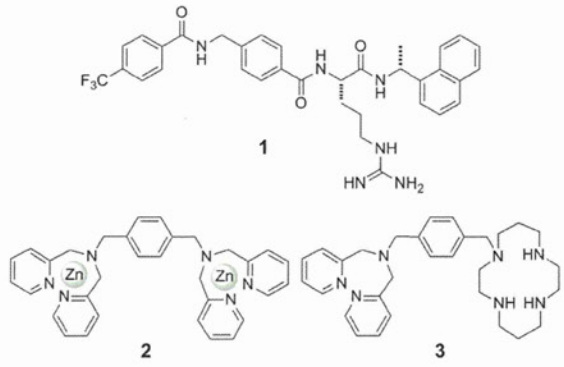

Figure 1. The structures of **1** (ST34), Dpa-Zn complex (**2**) and Dpa-cyclam compound (**3**).

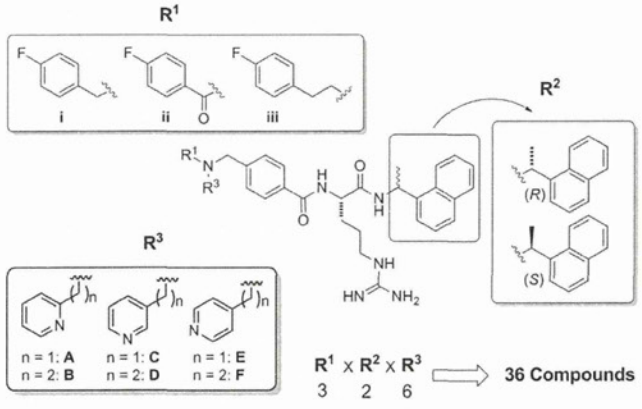

Figure 2. The structures of substituents for three parts of compound **1** in the design of new compounds.

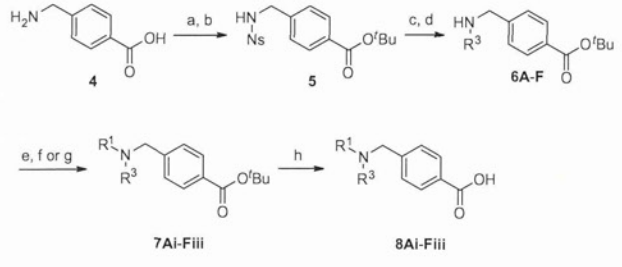

Scheme 1. The synthetic scheme of Unit 1, compounds **8Ai–Fiii**. Reagents and conditions and yields: (a) NsCl, Et_3N, THF/H_2O (1/1); (b) isobutene, THF/H_2SO_4 (10/1), 39% (2 steps); (c) PPh_3, DEAD, R^3OH, THF; (d) PhSH, K_2CO_3, DMF, 42–92% (2 steps); (e) $NaBH(OAc)_3$, 4-fluorobenzaldehyde, CH_2Cl_2; (f) $NaBH(OAc)_3$, (4-fluorophenyl)acetaldehyde, CH_2Cl_2; g) 4-fluorobenzoyl chloride, Et_3N, CH_2Cl_2, 51-94%; (h) TFA then 4 M HCl/EtOAc, quantitative; The structures of R^1 and R^3 are shown in Fig. 2 as i–iii and **A–F**, respectively. Ns = 2-nitrobenzenesulfonyl, ^{t}Bu = *tert*-butyl, DEAD = diethyl azodicarboxylate.

The synthesis of Unit 2 is shown in Scheme 2. Condensation of Boc-Arg(Mts)-OH (**9**) and (*R*)-1-naphthylethylamine or its (*S*) isomer produced amides (*R*)-**10** or (*S*)-**10**. Removal of the Boc group gave Unit 2, (*R*)-**11** and (*S*)-**11**.

Compounds **12–47** were synthesized by amide condensation of Unit 1, **8Ai–Fiii**, with Unit 2, (*R*)-**11** and (*S*)-**11**, and subsequent deprotection of the Mts group, as shown in Scheme 3.[15] All the synthetic compounds were purified by preparative reverse phase HPLC. In cases where peaks derived from side products appeared around the target peaks on the HPLC profile, the precise analysis was accomplished, giving rise to lower yields (Scheme 3, l).

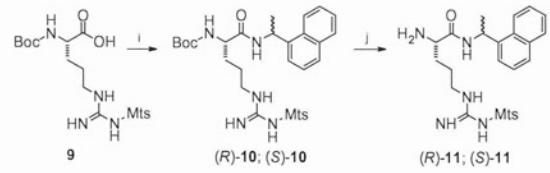

Scheme 2. Synthetic schemes of Unit 2, compounds (***R/S*)-11**. Reagents and conditions: (i) EDCI·HCl, $HOBt·H_2O$, Et_3N, (*R/S*)-(+/−)-1-(1-naphthyl)ethylamine, CH_2Cl_2, 83–97%; (j) TFA then 4 M HCl/EtOAc, quantitative; EDCI·HCl = 1-ethyl-3-(3-dimethylaminopropyl)carbodiimide hydrochloride, $HOBt·H_2O$ = 1-hydroxybenzotriazol monohydrate, Mts = 2,4,6-trimethylphenylsulfonyl, Boc = *tert*-butoxycarbonyl.

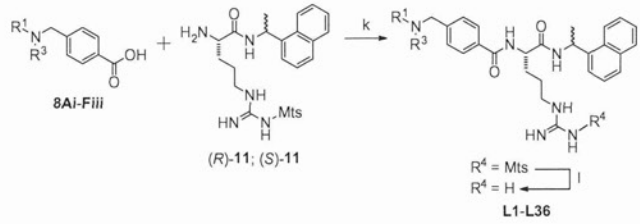

Scheme 3. Synthetic schemes of compounds **12–47**. Reagents and conditions: (k) EDCI·HCl, $HOBt·H_2O$, Et_3N, DMF, 36-95%; (l) TMSBr, *m*-cresol, 1,2-ethanedithiol, thioanisole, TFA, 4–54%. The structures of R^1 and R^3 are shown in Figure 2 as i–iii and **A–F**, respectively.

The CXCR4-binding activity of synthetic compounds was assessed in terms of the inhibition of [^{125}I]-CXCL12 binding to Jurkat cells, which express CXCR4.[16] The percent inhibition of all the compounds at 10 μM is shown in Table 1. Several of the compounds showed significant binding affinity. In general, compounds in which the 1-naphthylethylamine moiety (R^2) has the (*S*)-stereochemistry, as in KRH-1636, are more potent than the (*R*)-stereoisomers. Ten compounds (**26–28**, **30**, **33**, **36**, **39**, **44**, **45** and **47**, Table 1) were found to induce at least 30% inhibition and compounds **26**, **27** and **33**, which have a pyridyl group with a nitrogen atom at the β-position, showed more than 60% inhibition. It is noteworthy that compounds **26** and **27** in which R^2 is a (*R*)-1-naphthylethylamine moiety, are both more potent than the corresponding (*S*)-stereoisomers **44** and **45.** Compounds **26**, **27** and **33**, have a 4-fluorobenzyl or 4-fluorophenylethyl group, which rather than an amide, is a reductive alkyl type (R^1). As can be seen from Table 1, there is a tendency for compounds with a pyridyl group with a nitrogen atom at the β-position (R^3: C or D), to be more potent in terms of CXCR4-binding activity than the corresponding compounds, which have a pyridyl group with a nitrogen atom at the α- or γ- position (R^3: A, B, E or F), and those with a reductive alkyl 4-fluorobenzyl or 4-fluorophenylethyl group (R^1: i or iii), to be more potent in CXCR4-binding activity than the corresponding compounds, with a 4-fluorobenzoyl group (R^1: ii).

Compounds were next evaluated for anti-HIV activity and cytotoxicity. CXCR4 is the major co-receptor for the entry of T-cell line-tropic (X4-) HIV-1.[5] Accordingly, inhibitory activity against X4-HIV-1 (NL4-3 strain)-induced cytopathogenicity in MT-4 cells (anti-HIV activity), and reduction of the viability in MT-4 cells (cytotoxicity) were assessed[16] and are shown in Table 1. Compounds **26** and **33–35** showed significant anti-HIV activity with EC_{50} values in the micromolar range. Compounds **26** and **33** showed both potent CXCR4-binding activity (79% and 60% inhibition at 10 μM, respectively) and anti-HIV activity (EC_{50} = 11 and 13 μM, respectively), the two activities being highly correlated. Compounds **34** and **35** have significant anti-HIV activity with EC_{50} values of 8 and 10 μM, respectively, which is higher than CXCR4-binding activities, which are 16% and 20% inhibition at 10 μM, respectively. Compound **27**, which showed relatively high CXCR4-binding activity (69% inhibition at 10 μM), failed to show

Table 1
CXCR4-binding activity, anti-HIV activity and cytotoxicity of compounds **12–47**

Compd no.	R^1 [a]	R^2 [b]	R^3 [c]	Inhibition[d] (%)	EC_{50}[e] (μM)	CC_{50}[f] (μM)	Compd no.	R^1 [a]	R^2 [b]	R^3 [c]	Inhibition[d] (%)	EC_{50}[e] (μM)	CC_{50}[f] (μM)
12	i	(*R*)	A	0	>20	35	**30**	i	(*S*)	A	30 ± 1.1	>4	11
13	i	(*R*)	B	4 ± 1.7	>4	23	**31**	i	(*S*)	B	25 ± 3.3	>20	24
14	i	(*R*)	C	6 ± 0.7	>20	37	**32**	i	(*S*)	C	27 ± 1.7	>20	41
15	i	(*R*)	D	24 ± 1.7	n.d.	n.d.	**33**	i	(*S*)	D	60 ± 1.5	13	65
16	i	(*R*)	E	12 ± 3.0	>20	39	**34**	i	(*S*)	E	16 ± 1.2	8	44
17	i	(*R*)	F	16 ± 2.2	n.d.	n.d.	**35**	i	(*S*)	F	20 ± 1.3	10	44
18	ii	(*R*)	A	3 ± 0.9	>20	38	**36**	ii	(*S*)	A	36 ± 1.8	>20	37
19	ii	(*R*)	B	6 ± 3.9	>20	41	**37**	ii	(*S*)	B	0	>20	43
20	ii	(*R*)	C	11 ± 0.8	>20	45	**38**	ii	(*S*)	C	14 ± 1.4	>20	57
21	ii	(*R*)	D	22 ± 4.1	n.d.	n.d.	**39**	ii	(*S*)	D	32 ± 8.4	n.d.	n.d.
22	ii	(*R*)	E	6 ± 2.7	>20	45	**40**	ii	(*S*)	E	13 ± 15	>20	51
23	ii	(*R*)	F	12 ± 1.9	n.d.	n.d.	**41**	ii	(*S*)	F	25 ± 13	>20	47
24	iii	(*R*)	A	15 ± 2.1	n.d.	n.d.	**42**	iii	(*S*)	A	16 ± 5.1	>4	9.9
25	iii	(*R*)	B	13 ± 0.6	>20	27	**43**	iii	(*S*)	B	23 ± 14	>4	13
26	iii	(*R*)	C	79 ± 14	11	47	**44**	iii	(*S*)	C	36 ± 13	n.d.	n.d.
27	iii	(*R*)	D	69 ± 5.0	>11	11	**45**	iii	(*S*)	D	35 ± 5.2	n.d.	n.d.
28	iii	(*R*)	E	44 ± 5.4	n.d.	n.d.	**46**	iii	(*S*)	E	26 ± 23	n.d.	n.d.
29	iii	(*R*)	F	0	n.d.	n.d.	**47**	iii	(*S*)	F	51 ± 6.6	n.d.	n.d.
KRH-1636				100	0.33	80	FC131				100	0.16	>10
AMD3100				n.d.	0.062	55	1 (ST34)				n.d.	7.4	66
AZT				n.d.	0.058	100							

[a,c] The structures of R^1 and R^3 are shown in Fig. 2 as i–iii and **A–F**, respectively.
[b] The absolute configuration in stereochemistry of R^2 shown in Fig. 2 is described.
[d] CXCR4-binding activity was assessed based on the inhibition of the [^{125}I]-CXCL12 binding to Jurkat cells. Inhibition percentages of all the compounds at 10 μM were calculated relative to the inhibition percentage by T140 (100%).
[e] EC_{50} values are the concentrations for 50% protection from X4-HIV-1 (NL4-3 strain)-induced cytopathogenicity in MT-4 cells.
[f] CC_{50} values are the concentrations for 50% reduction of the viability of MT-4 cells. All data are the mean values from at least three independent experiments.

significant anti-HIV activity at concentrations below 11 μM because of high cytotoxicity (CC_{50} = 11 μM). With the exception of **27**, **30**, **42** and **43**, the tested compounds showed no significant cytotoxicity (CC_{50} >20 μM, Table 1). On the other hand, compounds **26**, **27**, **33**, **34** and **35** at concentrations below 100 μM failed to show significant protective activity against macrophage-tropic (R5-) HIV-1 (NL(AD8) strain)-induced cytopathogenicity in PM-1/CCR5, whereas the EC_{50} of the CCR5 antagonist SCH-D[17] in this assay was 0.055 μM (data not shown). Since instead of CXCR4, R5-HIV-1 strains use the chemokine receptor CCR5, a member of the GPCR family, as the major co-receptor for their entry, this suggests that these compounds do not bind to CCR5. Thus, compounds **26**, **27**, **33**, **34** or **35** have highly selective affinity for CXCR4. Compounds **34** and **35**, which have significant anti-HIV activity, have a pyridyl group with a nitrogen atom at the γ-position, in contrast to compounds **26**, **27** and **33** which also show CXCR4-binding activity, but have a pyridyl group with a nitrogen atom at the β-position. Furthermore, compounds **34** and **35** have R^1 = 4-fluorobenzyl and R^2 = (*S*)-1-naphthylethylamine. A possible explanation of these observations is that compounds **34** and **35** compete with HIV-1 in binding to CXCR4 while compounds **26** and **33** compete with HIV-1 and CXCL12. Compound **27** does not compete with HIV-1 because of its high cytotoxicity. This suggests that the CXCR4 binding site used by compounds **34** and **35** differs slightly from that used by compounds **26**, **27** and **33**.

Low molecular weight CXCR4 ligands with two types of recognition modes for CXCR4 have been obtained in this study: one causes competition with HIV-1 on CXCR4 whereas the other causes competition with HIV-1 and CXCL12. These compounds have selective affinity for CXCR4 because they do not significantly bind to CCR5. Further structural modification studies of these CXCR4 ligands are the subject of an ongoing project.

Acknowledgements

This work was supported by Grant-in-Aid for Scientific Research from the Ministry of Education, Culture, Sports, Science, and Technology of Japan, Japan Human Science Foundation, and Health and Labour Sciences Research Grants from Japanese Ministry of Health, Labor, and Welfare. T.T. and C.H. are grateful for the JSPS Research Fellowships for Young Scientists.

References and notes

1. (a) Nagasawa, T.; Kikutani, H.; Kishimoto, T. *Proc. Natl. Acad. Sci. U. S. A.* **1994**, *91*, 2305; (b) Bleul, C. C.; Farzan, M.; Choe, H.; Parolin, C.; Clark-Lewis, I.; Sodroski, J.; Springer, T. A. *Nature* **1996**, *382*, 829; (c) Oberlin, E.; Amara, A.; Bachelerie, F.; Bessia, C.; Virelizier, J. L.; Arenzana-Seisdedos, F.; Schwartz, O.; Heard, J. M.; Clark-Lewis, I.; Legler, D. L.; Loetscher, M.; Baggiolini, M.; Moser, B. *Nature* **1996**, *382*, 833; (d) Tashiro, K.; Tada, H.; Heilker, R.; Shirozu, M.; Nakano, T.; Honjo, T. *Science* **1993**, *261*, 600.
2. Bleul, C. C.; Fuhlbrigge, R. C.; Casanovas, J. M.; Aiuti, A.; Springer, T. A. *J. Exp. Med.* **1996**, *2*, 1101.
3. (a) Tachibana, K.; Hirota, S.; Iizasa, H.; Yoshida, H.; Kawabata, K.; Kataoka, Y.; Kitamura, Y.; Matsushima, K.; Yoshida, N.; Nishikawa, S.; Kishimoto, T.; Nagasawa, T. *Nature* **1998**, *393*, 591; (b) Nagasawa, T.; Hirota, S.; Tachibana, K.; Takakura, N.; Nishikawa, S.; Kitamura, Y.; Yoshida, N.; Kikutani, H.; Kishimoto, T. *Nature* **1996**, *382*, 635.
4. (a) Zhu, Y.; Yu, Y.; Zhang, X. C.; Nagasawa, T.; Wu, J. Y.; Rao, Y. *Nat. Neurosci.* **2002**, *5*, 719; (b) Stumm, R. K.; Zhou, C.; Ara, T.; Lazarini, F.; Dubois-Dalcq, M.; Nagasawa, T.; Hollt, V.; Schulz, S. *J. Neurosci.* **2003**, *23*, 5123.
5. (a) Deng, H. K.; Liu, R.; Ellmeier, W.; Choe, S.; Unutmaz, D.; Burkhart, M.; Marzio, P. D.; Marmon, S.; Sutton, R. E.; Hill, C. M.; Davis, C. B.; Peiper, S. C.; Schall, T. J.; Littman, D. R.; Landau, N. R. *Nature* **1996**, *381*, 661; (b) Feng, Y.; Broder, C. C.; Kennedy, P. E.; Berger, E. A. *Science* **1996**, *272*, 872.
6. (a) Koshiba, T.; Hosotani, R.; Miyamoto, Y.; Ida, J.; Tsuji, S.; Nakajima, S.; Kawaguchi, M.; Kobayashi, H.; Doi, R.; Hori, T.; Fujii, N.; Imamura, M. *Clin. Cancer. Res.* **2000**, *6*, 3530; (b) Müller, A.; Homey, B.; Soto, H.; Ge, N.; Catron, D.; Buchanan, M. E.; McClanahan, T.; Murphy, E.; Yuan, W.; Wagner, S. N.; Barrera, J. L.; Mohar, A.; Verastegui, E.; Zlotnik, A. *Nature* **2001**, *410*, 50; (c) Tamamura, H.; Hori, A.; Kanzaki, N.; Hiramatsu, K.; Mizumoto, M.; Nakashima, H.; Yamamoto, N.; Otaka, A.; Fujii, N. *FEBS Lett.* **2003**, *550*, 79.
7. (a) Tsukada, N.; Burger, J. A.; Zvaifler, N. J.; Kipps, T. J. *Blood* **2002**, *99*, 1030; (b) Juarez, J.; Bradstock, K. F.; Gottlieb, D. J.; Bendall, L. J. *Leukemia* **2003**, *17*, 1294.
8. (a) Nanki, T.; Hayashida, K.; El-Gabalawy, H. S.; Suson, S.; Shi, K.; Girschick, H. J.; Yavuz, S.; Lipsky, P. E. . *J. Immunol.* **2000**, *165*, 6590; (b) Tamamura, H.; Fujisawa, M.; Hiramatsu, K.; Mizumoto, M.; Nakashima, H.; Yamamoto, N.; Otaka, A.; Fujii, N. *FEBS Lett.* **2004**, *569*, 99.
9. (a) Murakami, T.; Nakajima, T.; Koyanagi, Y.; Tachibana, K.; Fujii, N.; Tamamura, H.; Toshida, N.; Waki, M.; Matsumoto, A.; Yoshie, O.; Kishimoto, T.; Yamamoto, N.; Nagasawa, T. *J. Exp. Med.* **1997**, *186*, 1389; (b) Tamamura, H.; Xu, Y.; Hattori, T.; Zhang, X.; Arakaki, R.; Kanbara, K.; Omagari, A.; Otaka, A.; Ibuka, T.; Yamamoto, N.; Nakashima, H.; Fujii, N. *Biochem. Biophys. Res.*

Commun. **1998**, *253*, 877; (c) Tamamura, H.; Omagari, A.; Oishi, S.; Kanamoto, T.; Yamamoto, N.; Peiper, S. C.; Nakashima, H.; Otaka, A.; Fujii, N. *Bioorg. Med. Chem. Lett.* **2000**, *10*, 2633; (d) Fujii, N.; Oishi, S.; Hiramatsu, K.; Araki, T.; Ueda, S.; Tamamura, H.; Otaka, A.; Kusano, S.; Terakubo, S.; Nakashima, H.; Broach, J. A.; Trent, J. O.; Wang, Z.; Peiper, S. C. *Angew. Chem., Int. Ed.* **2003**, *42*, 3251; (e) Tamamura, H.; Hiramatsu, K.; Ueda, S.; Wang, Z.; Kusano, S.; Terakubo, S.; Trent, J. O.; Peiper, S. C.; Yamamoto, N.; Nakashima, H.; Otaka, A.; Fujii, N. *J. Med. Chem.* **2005**, *48*, 380; (f) Tamamura, H.; Araki, T.; Ueda, S.; Wang, Z.; Oishi, S.; Esaka, A.; Trent, J. O.; Nakashima, H.; Yamamoto, N.; Peiper, S. C.; Otaka, A.; Fujii, N. *J. Med. Chem.* **2005**, *48*, 3280; (g) Hashimoto, C.; Tanaka, T.; Narumi, T.; Nomura, W.; Tamamura, H. *Expert Opin. Drug Disc.* **2011**, *6*, 1067.

10. Tamamura, H.; Tsutsumi, H.; Masuno, H.; Mizokami, S.; Hiramatsu, K.; Wang, Z.; Trent, J. O.; Nakashima, H.; Yamamoto, N.; Peiper, S. C.; Fujii, N. *Org. Biomol. Chem.* **2006**, *4*, 2354.
11. Schols, D.; Struyf, S.; Van Damme, J.; Este, J. A.; Henson, G.; DeClarcq, E. *J. Exp. Med.* **1997**, *186*, 1383.
12. Ichiyama, K.; Yokoyama-Kumakura, S.; Tanaka, Y.; Tanaka, R.; Hirose, K.; Bannai, K.; Edamatsu, T.; Yanaka, M.; Niitani, Y.; Miyano-Kurosaki, N.; Takaku, H.; Koyanagi, Y.; Yamamoto, N. *Proc. Natl. Acad. Sci. U.S.A.* **2003**, *100*, 4185.
13. Tamamura, H.; Ojida, A.; Ogawa, T.; Tsutsumi, H.; Masuno, H.; Nakashima, H.; Yamamoto, N.; Hamachi, I.; Fujii, N. *J. Med. Chem.* **2006**, *49*, 3412.
14. Tanaka, T.; Narumi, T.; Ozaki, T.; Sohma, A.; Ohashi, N.; Hashimoto, C.; Itotani, K.; Nomura, W.; Murakami, T.; Yamamoto, N.; Tamamura, H. *ChemMedChem* **2011**, *6*, 834.
15. *For example, the synthesis of compound* ***30***: To a stirred solution of **8Ai** (176 mg, 0.415 mmol, HCl salt) in DMF (4 mL) were added EDCI·HCl (104 mg, 0.454 mmol), HOBt·H_2O (58.4 mg, 0.381 mmol), Et_3N (301 μL, 2.16 mmol) and ***(S)*-11** (320 mg, 0.657 mmol, HCl salt) at 0 °C. The mixture was stirred at room temperature for 43 h. The reaction mixture was diluted with $CHCl_3$ and washed with saturated citric acid, saturated $NaHCO_3$ and brine, and dried over $MgSO_4$. Concentration under reduced pressure followed by flash column chromatography over silica gel with $CHCl_3$/MeOH (20/1) gave the condensation product (175 mg, 0.208 mmol, 50% yield) as white powder. To this compound were added *m*-cresol (75.0 μL, 0.714 mmol), 1,2-ethanedithiol (225 μL, 2.68 mmol), thioanisole (225 μL, 1.91 mmol), TFA (3 mL) and bromotrimethylsilane (495 μL, 3.82 mmol) with stirring at 0 °C, and the stirring was continued at room temperature for 3.5 h under N_2. The reaction mixture was concentrated under reduced pressure, followed by addition of Et_2O to precipitate the product. After washing with Et_2O, the crude product was purified by preparative HPLC and lyophilized to give the compound **30** (15.6 mg, 0.0236 mmol, 13%) as white powder. ^1H NMR δ_H (400 MHz; DMSO-d_6) 1.49 (m, 2H), 1.51 (d, J = 7.2 Hz, 3H), 1.80–1.62 (m, 2H), 3.07 (dd, J = 6.4, 12.8 Hz, 2H), 3.85 (s, 2H), 3.91 (s, 4H), 4.54 (m, 1H), 5.72 (m, 1H), 7.13 (t, J = 8.8 Hz, 2H), 7.40 (m, 1H), 7.60–7.45 (m, 10H), 7.75–7.95 (m, 5H), 8.10 (m, 1H), 8.40 (d, J = 8.0 Hz, 1H), 8.58 (m, 1H), 8.65 (d, J = 7.6 Hz, 1H); LRMS (ESI), m/z calcd for $C_{39}H_{42}FN_7O_2$ $(MH)^+$ 660.34, found 660.31.
16. Tanaka, T.; Tsutsumi, H.; Nomura, W.; Tanabe, Y.; Ohashi, N.; Esaka, A.; Ochiai, C.; Sato, J.; Itotani, K.; Murakami, T.; Ohba, K.; Yamamoto, N.; Fujii, N.; Tamamura, H. *Org. Biomol. Chem.* **2008**, *6*, 4374.
17. Tagat, J. R.; McCombie, S. W.; Nazareno, D.; Labroli, M. A.; Xiao, Y.; Steensma, R. W.; Strizki, J. M.; Baroudy, B. M.; Cox, K.; Lachowicz, J.; Varty, G.; Watkins, R. *J. Med. Chem.* **2004**, *47*, 2405.

JVI
Journals.ASM.org

Reevaluation of the Requirement for TIP47 in Human Immunodeficiency Virus Type 1 Envelope Glycoprotein Incorporation

Mary Ann Checkley,[a] Benjamin G. Luttge,[a] Peter Y. Mercredi,[b] Sampson K. Kyere,[b] Justin Donlan,[b] Tsutomu Murakami,[c] Michael F. Summers,[b] Simon Cocklin,[d] Eric O. Freed[a]

Virus-Cell Interaction Section, HIV Drug Resistance Program, Center for Cancer Research, National Cancer Institute, Frederick National Laboratory for Cancer Research, Frederick, Maryland, USA[a]; Howard Hughes Medical Institute, Department of Chemistry and Biochemistry, University of Maryland, Baltimore County, Baltimore, Maryland, USA[b]; AIDS Research Center, National Institute of Infectious Diseases, Shinjuku, Tokyo, Japan[c]; Department of Biochemistry and Molecular Biology, Drexel University College of Medicine, Philadelphia, Pennsylvania, USA[d]

Incorporation of the human immunodeficiency virus type 1 (HIV-1) envelope glycoproteins into assembling particles is crucial for virion infectivity. Genetic and biochemical data indicate that the matrix (MA) domain of Gag and the cytoplasmic tail of the transmembrane glycoprotein gp41 play an important role in coordinating Env incorporation; however, the molecular mechanism and possible role of host factors in this process remain to be defined. Recent studies suggested that Env incorporation is mediated by interactions between matrix and tail-interacting protein of 47 kDa (TIP47; also known as perilipin-3 and mannose-6-phosphate receptor-binding protein 1), a member of the perilipin, adipophilin, TIP47 (PAT) family of proteins implicated in protein sorting and lipid droplet biogenesis. We have confirmed by nuclear magnetic resonance spectroscopy titration experiments and surface plasmon resonance that MA binds TIP47. We also reevaluated the role of TIP47 in HIV-1 Env incorporation in HeLa cells and in the Jurkat T-cell line. In HeLa cells, TIP47 overexpression or RNA interference (RNAi)-mediated depletion had no significant effect on HIV-1 Env incorporation, virus release, or particle infectivity. Similarly, depletion of TIP47 in Jurkat cells did not impair HIV-1 Env incorporation, virus release, infectivity, or replication. Our results thus do not support a role for TIP47 in HIV-1 Env incorporation or virion infectivity.

Incorporation of the Env glycoprotein complex into assembling HIV-1 particles is critical for viral infectivity and replication. Env is synthesized as an ~160-kDa precursor polyprotein (gp160) in the endoplasmic reticulum (ER) and is processed into the mature surface glycoprotein gp120 and transmembrane glycoprotein gp41 during transport to virus assembly sites on the plasma membrane (1). Although many aspects of the HIV-1 assembly pathway have been deciphered over the past 2 decades (2, 3), the mechanism of Env recruitment and incorporation remains poorly understood. Several non-mutually exclusive models for Env incorporation have been suggested (1, 4): (i) an active model, in which Env is recruited through a direct interaction with the viral structural polyprotein Gag; (ii) a passive model, in which Env present at assembly sites is randomly incorporated; (iii) a Gag-Env cotargeting model, in which both Gag and Env localize to a common membrane microdomain to increase the local concentration of viral proteins at assembly sites; and (iv) an indirect Gag-Env interaction model, in which Env incorporation requires the formation of a ternary complex composed of Env, Gag, and a host cellular factor. The active model is supported by studies showing that mutations in the matrix protein (MA) or the gp41 cytoplasmic tail (CT) reduce levels of incorporation and that second-site compensatory mutations in MA can rescue other MA substitutions or a small gp41 CT deletion that blocks Env incorporation (5–11). The passive model for Env incorporation derives support from pseudotyping experiments, wherein foreign (non-HIV-1) or HIV-1 CT-deleted viral Env glycoproteins are incorporated into HIV-1 particles in the presumed absence of a direct Gag-Env interaction (12, 13). The colocalization of Gag and Env in cholesterol-enriched plasma membrane microdomains (lipid rafts) that become part of the virion lipid bilayer is consistent with the Gag-Env cotargeting model (14).

The indirect Gag-Env interaction model posits that a host factor interacts with MA and/or the gp41 CT to promote Env incorporation. The observation that truncation of the gp41 CT blocks Env incorporation in most T-cell lines and in primary cell types (T cells and monocyte-derived macrophages) but has only a modest effect in several laboratory cell lines (15, 16) supports the notion that a host factor(s) bridges MA and the gp41 CT to recruit Env into particles. Recent studies suggested that tail-interacting protein of 47 kDa (TIP47) may serve such a bridging role (17–19): HIV-1 Gag and TIP47 coimmunoprecipitated in an *in vivo* pulldown assay; TIP47-MA binding was detectable *in vitro* in a quantitative yeast two-hybrid assay and in glutathione *S*-transferase (GST) pulldowns; TIP47 overexpression in HeLa cells increased Env incorporation into virions; depletion of TIP47 in cell-based assays decreased Env packaging; and MA and gp41 CT mutations that impair TIP47 binding reduced Env incorporation (17–19).

TIP47 is a soluble protein that forms oligomers in solution, a process promoted by 11-mer helix repeat elements within its ~150 N-terminal residues. These N-terminal residues do not appear to be required for TIP47 binding to cellular partners (e.g., mannose 6-phosphate receptors [M6PRs]), but they are required for function (20, 21). TIP47 was originally proposed to mediate the trafficking of M6PRs from late endosomes to the *trans*-Golgi network by selectively binding the cytoplasmic domains of these

Received 29 November 2012 Accepted 8 January 2013
Published ahead of print 16 January 2013
Address correspondence to Eric O. Freed, efreed@nih.gov.

doi:10.1128/JVI.03299-12

cargo receptors (21–24). More-recent phylogenetic, structural, and protein function studies indicated that TIP47 is a member of the perilipin/ADRP/TIP47 (PAT) protein family (20, 25). PAT proteins bind intracellular lipids either constitutively or in response to metabolic stimuli and are important in lipid droplet biogenesis (20, 25–27). X-ray crystallographic studies revealed that the C-terminal domain of TIP47 has a structure similar to that of the N-terminal domain of apolipoprotein E, suggesting a role for TIP47 in protein recruitment to lipid droplets and lipid biogenesis (20). TIP47 adopts an extended conformation in solution, suggesting that N- and C-terminal domains are well separated, perhaps facilitating independent functions of the two terminal regions (28).

To understand further the role of TIP47 in HIV-1 MA binding and Env incorporation, we have cloned, expressed, and purified the intact TIP47 protein and deletion mutants lacking the N terminus. Nuclear magnetic resonance (NMR) spectroscopy-detected titration experiments were performed with myristylated (myr) and unmyristylated [myr(−)] forms of HIV-1 MA. Surface plasmon resonance (SPR) assays were also performed to evaluate MA-TIP47 binding. Our results confirm that TIP47 binds MA and, contrary to expectations based on TIP47-M6PR binding (21), suggest that the N terminus of TIP47 is required for this interaction. However, we were unable to verify a role for TIP47 in HIV-1 Env glycoprotein incorporation into virions.

MATERIALS AND METHODS

Sample preparation for NMR. The DNAs encoding a C-terminally His-tagged TIP47 (residues 1 to 434) and a C-terminally His-tagged TIP47 fragment from which the N-terminal 112 residues were deleted (Δ1–112 TIP47), were subcloned and transformed into Rosetta 2 (DE3) pLysS expression cells (Novagen). Cells were grown in flasks of Luria broth medium, and unlabeled TIP47 and Δ1–112 TIP47 were induced with 1 mM isopropyl β-D-1-thiogalactopyranoside (IPTG) at an A_{600} reading of 0.6. The cells were harvested and lysed with a microfluidizer (Microfluidics) and clarified by centrifugation, and the target protein was applied to a cobalt affinity resin (BD Biosciences). The resin was washed extensively (50 mM sodium phosphate, pH 7.0, 500 mM sodium chloride, 5 mM dithiothreitol [DTT], 10 mM imidazole), and the proteins were eluted with wash buffer containing 250 mM imidazole. Gel filtration chromatography was used to purify the proteins to homogeneity (GE Healthcare). Electrospray mass spectrometry results indicated calculated molecular masses of 36,088.6 Da for Δ1-112 TIP47 and 47855.7 Da for intact TIP47. ^{15}N isotopically labeled Δ1-112 TIP47 was overexpressed in M9 minimal medium supplemented with 99.9% enriched ^{15}N-ammonium chloride as the sole nitrogen source (Isotec) and purified as above. ^{15}N-labeled myristylated (myr) and unmyristylated (myr−) HIV-1 MA samples were prepared as previously described (29, 30). The purified TIP47 and MA samples were simultaneously exchanged into an NMR buffer consisting of 50 mM sodium phosphate [pH 7.0], 5 mM DTT, and 10% D_2O. Titrations with ^{15}N-labeled Δ1-112 TIP47 were collected at pH 5.5.

NMR spectroscopy. Two-dimensional (2D) ^{1}H, ^{15}N heteronuclear single quantum coherence (^{1}H-^{15}N HSQC) NMR titration data were obtained with a Bruker Avance 600 MHz NMR spectrometer equipped with a cryoprobe, using protein concentrations of 25 to 200 μM (35°C). Data were processed using NMRPIPE (31) and analyzed using NMRView (32).

Recombinant protein production and purification. The MA region of the HIV-1 *gag* gene was amplified from plasmid pLAI (a generous gift from E. Kilareski and B. Wigdahl, Drexel University College of Medicine), using primers designed to facilitate ligation-independent cloning into the vector pETHSUL.1 (LabLife) (33). This vector is designed for the insertion of genes of interest in frame with an N-terminal SUMO tag (33). The recombinant pETHSUL plasmid was verified for the presence of MA insert by restriction digestion and sequence analysis (Genewiz, Inc., South Plainfield, NJ). The resultant vector was designated pSUMO-MA. The purification of H6SUMO-Gag was achieved via immobilized metal affinity chromatography (IMAC) using a Talon cobalt resin affinity column (CloneTech Laboratories, Inc.). The *Escherichia coli* strain BL21(DE3) Codon+-RIL (Stratagene) was used for expression of H6SUMO-MA from pSUMO-MA. Two milliliters of LB, containing 100 μg/ml ampicillin and 50 μg/ml chloramphenicol, was inoculated with a single transformed colony, and the culture was allowed to grow at 37°C for 9 h. Twenty-five milliliters of the preculture was used to inoculate 50 ml of the autoinducing medium ZYP-5052 (34) containing 100 μg/ml ampicillin and 50 μg/ml chloramphenicol. The culture was grown at 30°C for 16 h. Cells were harvested by centrifugation at 3,000 rpm for 20 min at 4°C, and the pellet was resuspended in 10 ml phosphate-buffered saline (PBS) (Roche) containing 2.5 mM imidazole. Cells were lysed by sonication, and the supernatant was clarified by centrifugation at 10,000 rpm (SS-34, Sorvall RC 5C Plus) for 20 min at 4°C. The supernatant was removed and applied to a Talon cobalt resin affinity column (CloneTech Laboratories), previously equilibrated with PBS (Roche). Loosely bound proteins were removed via 7 column volumes of PBS containing 7.5 mM imidazole. Tightly associated proteins were eluted in 3 column volumes of PBS containing 250 mM imidazole. The eluates were then pooled and made 1 mM with respect to EDTA. To this pooled sample was added 10 μg of a recombinant His_6-tagged form of the catalytic domain (dtUD1) of the *Saccharomyces cerevisiae* SUMO hydrolase (33). Cleavage was allowed to proceed for 4 h at 18°C. Following cleavage, the sample was dialyzed at 4°C overnight against 2 liters of PBS to remove any imidazole. After dialysis, the dtUD1-catalyzed cleavage reaction was subjected to a second cobalt affinity purification using the Talon cobalt resin affinity column (CloneTech Laboratories). In this purification step, however, the cleaved MA protein passes straight through the column due to removal of the 6-histidine tag. Subsequently, the subtractively purified MA was dialyzed against 25 mM Tris-HCl [pH 8.0]–10% glycerol, at 4°C overnight. This dialyzed sampled was then filtered and loaded onto a 5-ml Hi-Trap Q HP (GE Healthcare). The flowthrough, containing the MA, was concentrated, flash frozen in liquid nitrogen, and stored at −80°C.

The human TIP47 gene was amplified from total cDNA generated from the CEM human T lymphoblastoid cell line using primers designed to facilitate ligation-independent cloning into the vector pETHSUL (33). TIP47 was expressed in *E. coli* BL21(DE3) Codon+-RIL (Stratagene) and purified by the subtractive purification methodology outlined by Hynson et al. (28). In addition to the full-length TIP47, an N-terminally truncated mutant of TIP47 was created, based on the work of Hickenbottom et al. (20). All vectors were verified by DNA sequencing. Expression and purification were carried out as for full-length TIP47.

The cytoplasmic tail of the cation-dependent (CD) mannose 6-phosphate receptor (M6PR) was produced from its expression vector (generously provided by Susanne Pfeffer, Stanford University) and purified as previously described (22, 35, 36). A C-terminally truncated mutant Rab9A GTPase (37) was overproduced from plasmid pET28b-Rab9(1–177), generously provided by E. J. Meehan (University of Alabama, Huntsville, AL). *E. coli* strain BL21(DE3) (Stratagene) harboring pET28b-Rab9(1–177) was grown in superbroth at 37°C. Overproduction of the His tag fusion protein was induced at an A_{600} of ~2.0 with 1 mM IPTG for 2 h. Rab9(1–177) was purified using the same protocol as that used for HIV-1 MA purification, except that all buffers contained 10 μM GTP (Sigma). The eluates from the purification were pooled and then dialyzed at 4°C overnight against 2 liters of PBS containing 10 μM GTP to remove excess imidazole. Protein was stored at 4°C until used.

SPR binding assays. Binding studies were performed at 25°C using a Biacore 3000 optical biosensor equipped with a CM4 research grade sensor chip. Immobilization of proteins to sensor surfaces was achieved using standard amine coupling methods. Analysis of the direct binding of the CD-M6PR cytoplasmic tail to full-length and mutant TIP47 was achieved by passage over surfaces to which the TIP47 proteins had been immobi-

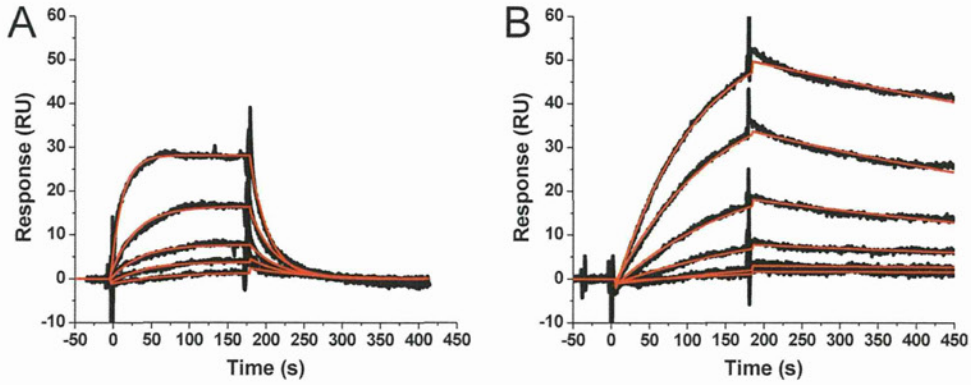

FIG 1 Interaction of purified TIP47 with its natural ligands in SPR assays. (A) Sensorgrams depicting the interaction of the cytoplasmic tail of CD-M6PR with sensor chip-immobilized human TIP47. Results for GST-tagged CD-M6PR cytoplasmic tail protein at concentrations of 0.134, 0.269, 0.538, 1.075, and 2.15 μM are shown. (B) Sensorgrams depicting the interaction of the Rab9 GTPase with sensor chip-immobilized human TIP47. Results for His-tagged Rab9(1–177) proteins at concentrations of 8.6, 17.3, 34.6, 134.3, and 276.6 nM are shown. Black lines indicate experimental data, whereas red lines indicate fitting to a 1:1 Langmuir binding model with a parameter included for mass transport. Kinetic values are as follows: for CD-M6PR-TIP47, $k_a = (1.3 \pm 0.2) \times 10^4\ M^{-1} \cdot s^{-1}$; $k_d = 4.5 \times 10^{-2} \cdot s^{-1}$; $K_D = 3.6$ μM; for Rab9-TIP47, $k_a = (4.2 \pm 2.0) \times 10^4\ M^{-1} \cdot s^{-1}$; $k_d = (1.0 \pm 0.1) \times 10^{-3} \cdot s^{-1}$; $K_D = 24.4$ nM.

lized directly using standard amine coupling. Different concentrations of CD-M6PR cytoplasmic tail diluted in PBS running buffer were passed over these surfaces at a flow rate of 50 μl/min for 3 min of association and 10 min of dissociation. Specific regeneration of the surfaces was not needed between injections due to the rapid dissociation rate. Analysis of the direct binding of the Rab9(1–177) protein was achieved by passage over surfaces to which the human TIP47 proteins had been immobilized directly. Different concentrations of Rab9(1–177) diluted in running buffer (PBS containing 10 μM GTP) were passed over these surfaces at a flow rate of 50 μl/min for 3 min of association and 10 min of dissociation. Specific regeneration of the surfaces between injections was achieved by pulses of 1.3 M NaCl–35 mM NaOH until the baseline returned to the preexposure value. For MA binding assays, different concentrations of MA, diluted in PBS running buffer, were passed over TIP47-containing surfaces at a flow rate of 50 μl/min for 3 min of association and 10 min of dissociation. Specific regeneration of the surfaces between injections was achieved by pulses of 10 mM glycine, pH 1.5, until the baseline returned to the preexposure value.

SPR data analysis was performed using BIAEvaluation 4.0 software (Biacore Inc., NJ). The responses of a buffer injection and responses from a reference flow cell were subtracted to account for nonspecific binding. Experimental data were fitted to a simple 1:1 binding model with a parameter included for mass transport. The average kinetic parameters (association [k_a[rsqb] and dissociation [k_d] rates) generated from a minimum of four data sets were used to define equilibrium association (K_A) and dissociation constants (K_D).

Cell culture, plasmids, transfections, and RNA interference (RNAi). Cell lines 293T, TZM-bl (obtained from J. Kappes through the NIH AIDS Research and Reference Reagent Program), and HeLa were maintained in Dulbecco's modified Eagle's medium (DMEM). Jurkat T cells were maintained in RPMI-1640 medium. All media were supplemented with 5 or 10% fetal bovine serum (FBS; HyClone), penicillin, and streptomycin unless otherwise indicated.

The full-length molecular clone pNL4-3 (38) was used in this study. Previous TIP47 studies (17, 19) used pHXB2R and pNL(AD8) clones. pNL(AD8) (39, 40) consists of pNL4-3 sequences encoding gp120 and the N-terminal portion (ectodomain) of gp41 from the CCR5-tropic clone pAD8. pNL(AD8) thus contains MA and gp41 cytoplasmic tail coding regions identical to (derived from) those of pNL4-3. pHXB2R and pNL4-3 are closely related molecular clones, and, importantly, are identical at residues implicated in TIP47 binding (residues 12, 15, 16, and 30 of MA and the YW motif in the gp41 CT) (19).

To deplete TIP47 in HeLa cells, 1×10^5 HeLa cells were transfected in suspension with 30 pmol of a pool of four TIP47 small interfering RNAs (siRNAs) (SMARTpool, Dharmacon) using RNAiMAX reagent (Invitrogen) and seeded in a 12-well plate in medium supplemented with 5% FBS. The next day, cells were transferred to a 6-well plate. Three days posttransfection with siRNA, cells were transfected with 3 μg of the pNL4-3 HIV-1

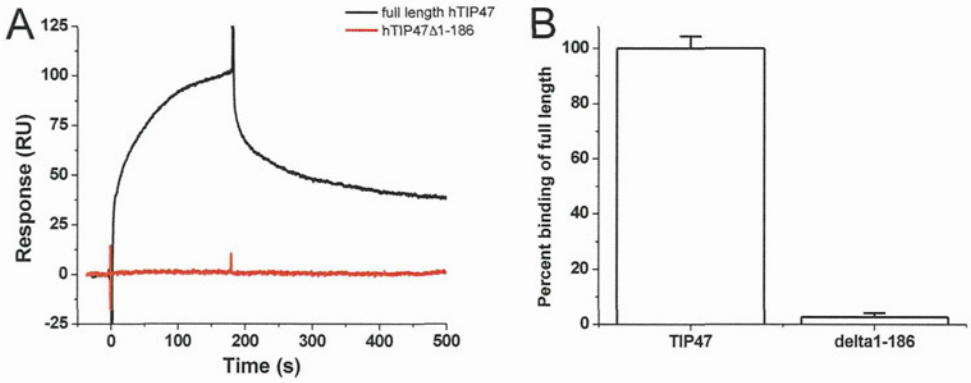

FIG 2 The N terminus of TIP47 is required for its interaction with HIV-1 MA in SPR assays. HIV-1 MA at a concentration of 250 nM was passed over full-length TIP47 and Δ1–186 TIP47, and the responses were recorded. (A) Representative sensorgrams for these interactions; (B) mean responses of three experiments in graphical form. Error bars represent 1 standard deviation.

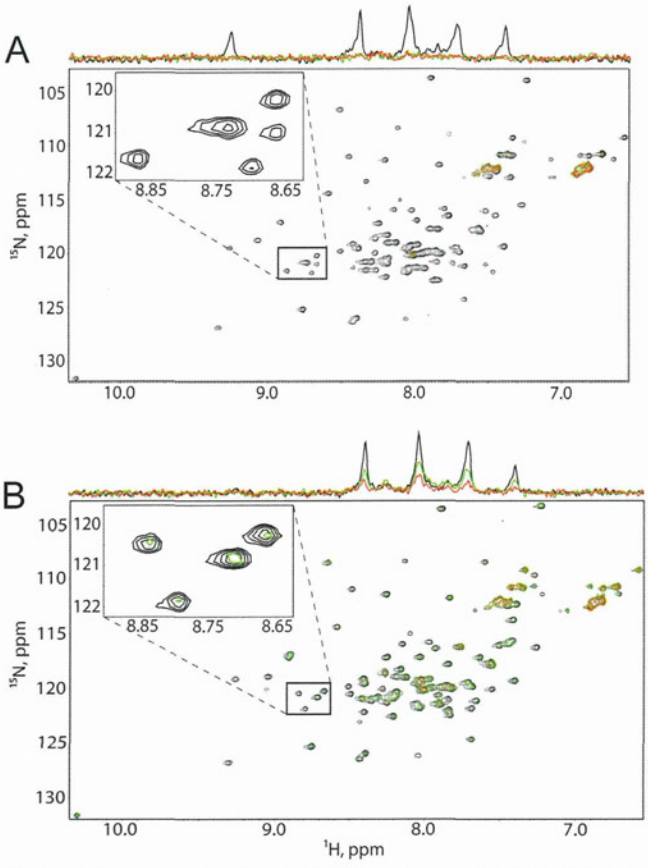

FIG 3 MA interacts with TIP47 in NMR-based assays. ^{1}H-^{15}N HSQC NMR spectra obtained upon titration of ^{15}N-labeled HIV-1 myrMA (50 μM) (A) and myr(−)MA (50 μM) (B) with intact TIP47; [TIP47]:[MA] = 0:1 (black), 0.5:1 (green), and 1:1 (red).

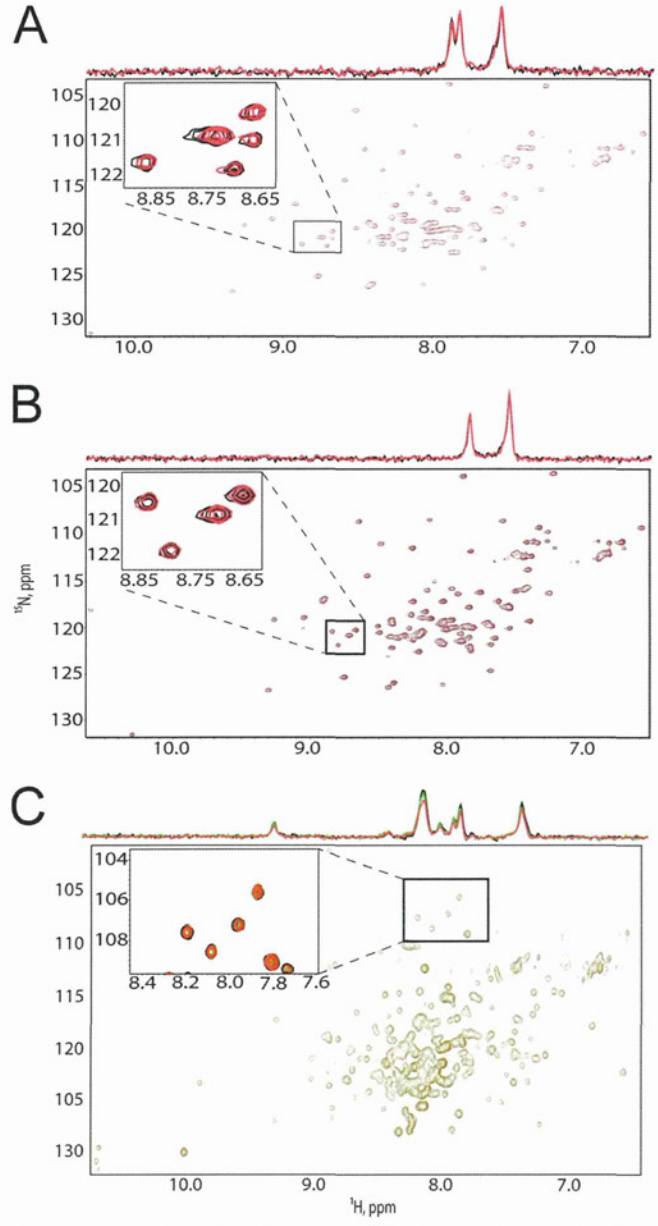

FIG 4 The N terminus of TIP47 is required for its interaction with TIP47 in NMR-based assays. (A, B) ^{1}H-^{15}N HSQC NMR spectra obtained for ^{15}N-labeled HIV-1 myrMA (50 μM) (A) and myr(−)MA (50 μM) (B) upon titration with Δ1–112 TIP47; [Δ1–112 TIP47]:[MA] = 0:1 (black), 1:1 (red). (C) ^{1}H-^{15}N HSQC NMR spectra obtained for ^{15}N-labeled Δ1–112 TIP47 upon titration with myrMA; [MA]:[Δ1–112 TIP47] = 0:1 (black), 2:1 (green), and 4:1 (red).

molecular clone (38) using Lipofectamine LTX (Invitrogen). Approximately 24 h posttransfection with pNL4-3, cells were metabolically radiolabeled with [^{35}S]Cys for 4 h. Virus-containing supernatants were filtered and subjected to ultracentrifugation (41, 42). Cell and virus lysates were immunoprecipitated with HIV immunoglobulin (HIV-Ig; obtained from the NIH AIDS Research and Reference Reagent Program) and analyzed by SDS-PAGE and fluorography. Bands were quantified by phosphorimager analysis using QuantityOne software (Bio-Rad).

To overexpress TIP47 in HeLa cells, 0.6 × 10^{6} HeLa cells were seeded on a 6-well plate. Cells were cotransfected with 2 μg of pNL4-3 and 0.5 or 1 μg of a plasmid containing the TIP47 open reading frame (ORF) driven by the cytomegalovirus (CMV) promoter (EX-U0354-MO2 from GeneCopoeia) or a green fluorescent protein (GFP)-expressing control plasmid (pmaxGFP from Lonza). Approximately 24 h postinfection, supernatants containing released virions were collected and cell and virus lysates were assayed for Env incorporation, virus release, and cellular levels of TIP47 as described above.

For short hairpin RNA (shRNA) transductions, five TIP47 MISSION shRNAs and the SCH002 nontargeting (NT) shRNA were obtained from Sigma: TRCN0000029679 NM_005817.2-904s1c1, TRCN0000029680 NM_005817.2-329s1c1, TRCN0000029681 NM_005817.2-1044s1c1, TRCN0000029682 NM_005817.2-1267s1c1, and TRCN0000029683 NM_005817.2-550s1c1, here referred to as TIP47 shRNAs 1, b, 2, c, and d, respectively. As a negative control, the SCH002 NT shRNA (Sigma) was used. C. Berlioz-Torrent (Institut Cochin, Paris, France) (19) kindly provided an anti-TIP47 shRNA pLKO.1-TIP1 (TIP1sensTRC sequence, CC GGAAGACTGTCTGCGACGCAGCACTCGAGTGCTGCGTCGCAGA CAGTCTTTTTTTG, and TIP1 antisenseTRC sequence, AATTCAAAAA AAGACTGTCTGCGACGCAGCACTCGAGTGCTGCGTCGCAGACA GTCTT), cloned into pLKO.1-TRC and here referred to as TIP47 shRNA 3. shRNAs were packaged in 293T cells by cotransfecting with pCMV delta R8.2 (43) and pHCMV-G (44) at a 1:1:0.1 ratio using Lipofectamine LTX reagent (Invitrogen) and a total of 2 μg DNA. Twenty-four hours posttransfection, media were changed, and virus-containing supernatant was collected 48 h posttransfection. To deplete TIP47 in the Jurkat T-cell line, 3 × 10^{5} Jurkat cells were infected with 50 to 75 μl of shRNA vector virus. Once cells had reached a density of 1 × 10^{6} cells/ml, shRNA-transduced cells were selected with 1 μg/ml of puromycin. From the five tested

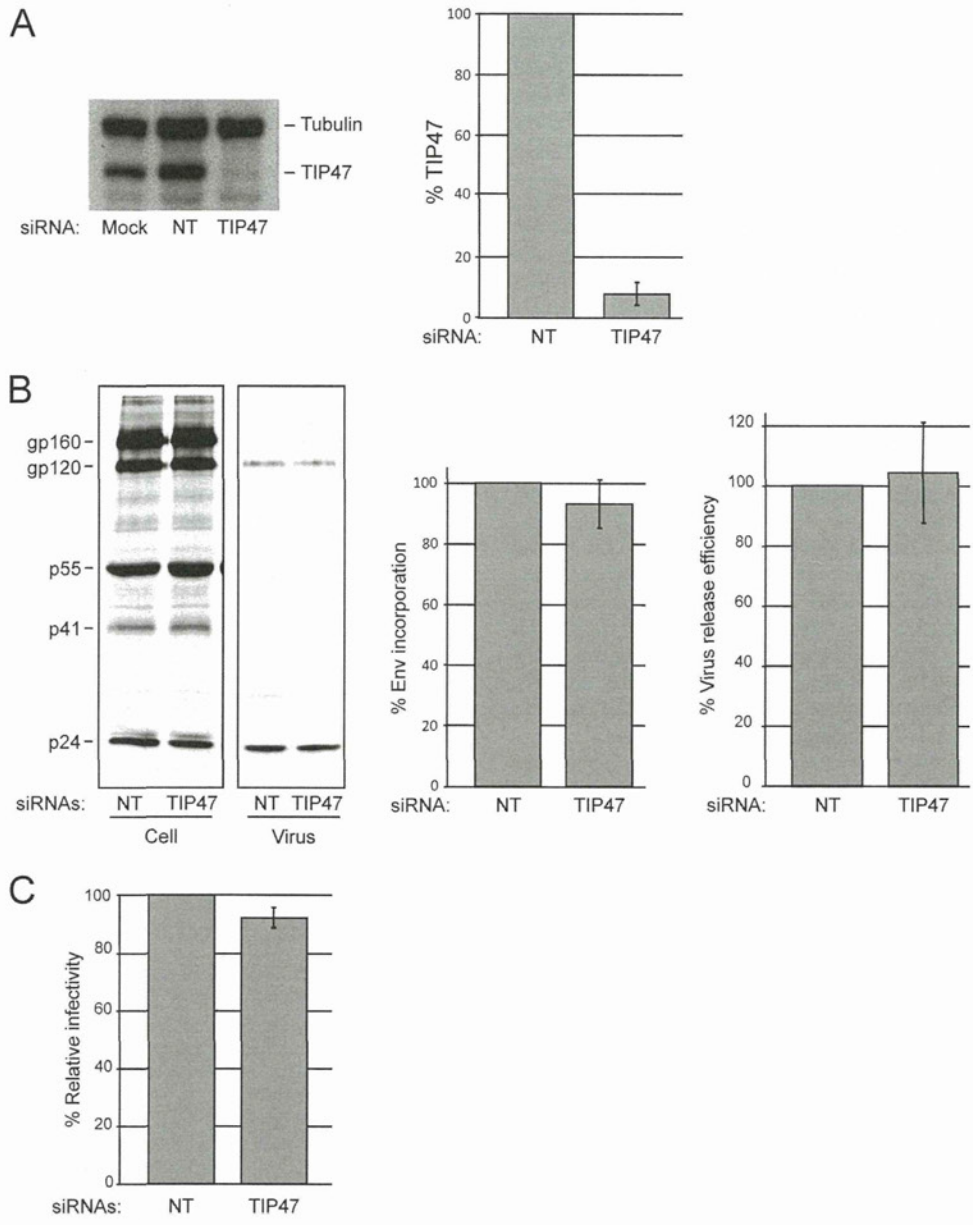

FIG 5 Depletion of TIP47 in HeLa cells does not impair HIV-1 Env incorporation, virus release, or infectivity in HeLa cells. Cells were transfected with 30 pmol nontargeting siRNA (NT) or a pool of four TIP47-specific siRNAs. (A) Transfected cell lysates were probed with antibodies specific for tubulin and TIP47 (left panel); the ratio of TIP47 to tubulin was quantified by using a FluorChem SP Imaging System (Alpha Innotech) (right panel) (means ± SD; $n = 3$). (B) Control and TIP47-depleted cells were transfected with pNL4-3 and metabolically radiolabeled with [^{35}S]Cys; cell and virus lysates were immunoprecipitated with HIV-Ig. The relative ratios of virus-associated gp120 to p24(CA) and virus release efficiencies were quantified by phosphorimager analysis (means ± SD; $n = 3$). (C) Virus-containing supernatants were harvested from control and TIP47-depleted cells, normalized for RT activity, and used to infect the TZM-bl indicator cell line. Graphs show average levels of infectivity with a virus input of 50,000 RT cpm. Luciferase activity was measured 2 days postinfection (means ± SD, $n = 3$).

shRNAs against TIP47, only two were found to consistently deplete TIP47. These two shRNAs were used independently to deplete TIP47 in all the experiments with Jurkat cells and were compared to the TIP1 (TIP47 3) shRNA (19). TIP47-depleted and NT-transduced Jurkat cells were infected with vesicular stomatitis virus (VSV)-G-pseudotyped HIV-1 prepared in 293T cells. Twenty-four hours postinfection, cell and virus lysates were assayed for Env incorporation, virus release, and cellular levels of TIP47 as described above.

Western blot analysis. Proteins were separated by SDS-PAGE (10% acrylamide) and transferred to polyvinylidene difluoride membranes using the iBlot Dry blotting system (Invitrogen). TIP47 protein was detected with goat anti-TIP47 IgG (sc-14723; Santa Cruz) at a 1:600 dilution, followed by horseradish peroxidase-conjugated mouse anti-goat IgG (Thermo Scientific). Alpha tubulin was detected with mouse anti-tubulin IgG (T6074; Sigma) at a 1:10,000 dilution, followed by horseradish peroxidase-conjugated goat anti-mouse IgG. Proteins were visualized by Western Lightning (Perkin-Elmer) and scanned using the FluorChem SP Imaging system (Alpha Innotech), followed by exposure to X-ray film. Levels of TIP47 and tubulin from cell lysates were quantified using Quantity One software (Bio-Rad). Standard deviations (SD) and standard errors of the mean (SEM) were calculated from at least three independent experiments.

RIPA analysis. Radioimmunoprecipitation assays (RIPA) were performed as previously described (41, 42, 45, 46). Approximately 18 h following transfection with pNL4-3 or infection with VSV-G-pseudotyped HIV-1, cells were washed and metabolically labeled in labeling medium (RPMI 1640 without L-Cys [MP Biomedicals no. 091646454] containing 5% FBS and 500 μCi [^{35}S]L-Cys /well) for 4 to 6 h at 37°C. Released virions were collected from culture supernatants by 0.45-μm filtration and ultracentrifugation at 125,000 × *g* for 45 min. Cell and virion samples were solubilized in lysis buffer (0.5% Triton X-100, 300 mM NaCl, 50 mM Tris [pH 7.5], and Complete protease inhibitor cocktail [Roche]). Cell lysates were precleared by adsorption with protein A agarose in RIPA buffer (0.1% Triton X-100, 300 mM NaCl, 50 mM Tris [pH 7.5]) and 0.1% bovine serum albumin (BSA). Virion and precleared cell lysates were immunoprecipitated at 4°C with HIV-Ig bound to protein A agarose beads. Immunoprecipitated cell lysates were washed three times with RIPA buffer and once with SDS-deoxycholic acid wash buffer (0.1% SDS, 300 mM NaCl, 50 mM Tris [pH 7.5], and 2.5 mM deoxycholic acid). Immunoprecipitated virus lysates were washed once with RIPA buffer. Immunoprecipitated proteins were eluted in Laemmli sample buffer at 99°C for 5 min and resolved by SDS-PAGE in 12% acrylamide with AcrylAide crosslinker (FMC Corp.). After fixation and dehydration of the gel, labeled proteins were detected by exposure to phosphor screens and quantified using Quantity One software (Bio-Rad). The percentage of Env incorporation was calculated as the amount of virion gp120 relative to the amount of virion capsid protein (CA). Virus release efficiency was calculated as the amount of virion CA over the total sum of cell and virion Gag ($Pr55^{Gag}$, p41, p25, and p24). Standard deviations and standard errors of the mean were calculated from at least three independent experiments.

Infectivity assays. Virus stocks used for infections were collected by 0.45-μm filtration of supernatant from transfected HeLa cells or infected Jurkat cells and then normalized for reverse transcriptase (RT) activity as previously described (42). For single-cycle infectivity assays, 5×10^4 TZM-bl cells/well were infected in the presence of 20 μg DEAE-dextran (GE Healthcare) per ml with four different virus inputs. Infected cells were lysed 48 h postinfection using Glo Lysis buffer (Promega) and assayed for luciferase activity using a luciferase assay kit (Promega) as previously described (47). Standard deviations and standard errors of the mean were calculated from at least three independent experiments.

Analysis of virus replication kinetics. To evaluate HIV-1 replication kinetics, 2×10^6 Jurkat cells were transfected with 2 μg of pNL4-3 in 200 μl of 0.7 mg/ml of DEAE-dextran and incubated for 15 min at 37°C. Cells were then washed with transfection buffer (25 mM Tris-HCl [pH 7.4], 0.6 mM Na_2HPO_4, 5 mM KCl, 140 mM NaCl, 0.7 mM $CaCl_2$, 0.5 mM $MgCl_2$) and resuspended in 1 ml of RPMI 1640 supplemented with 10% FBS. Cultures were split 1:3 every 2 to 3 days, at which time culture supernatants were collected to monitor RT activity (41).

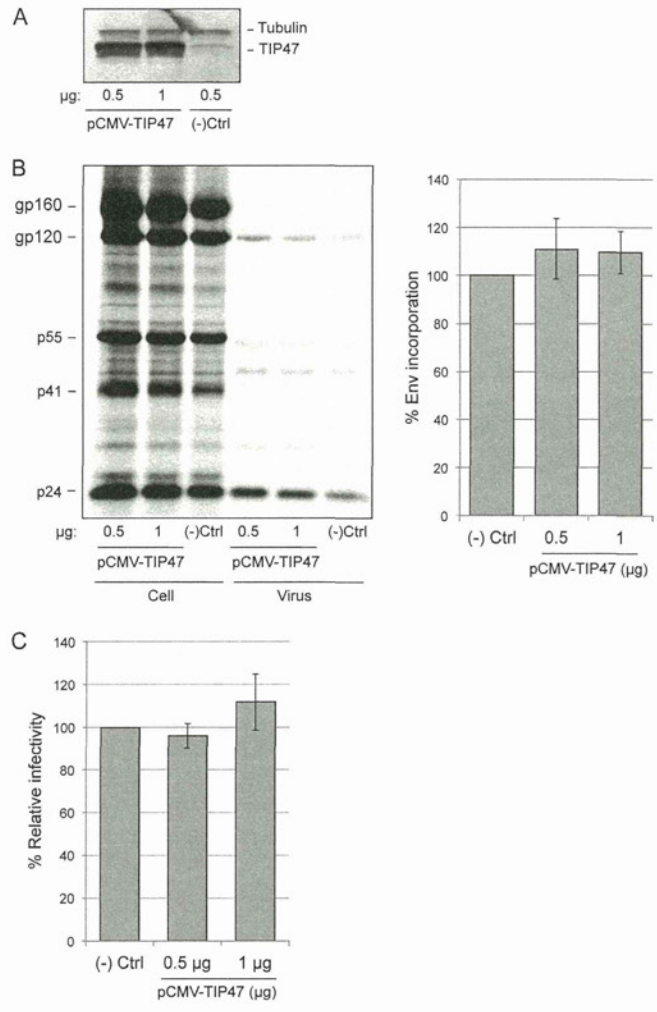

FIG 6 Overexpression of TIP47 in HeLa cells does not enhance HIV-1 Env incorporation or virion infectivity. HeLa cells were cotransfected with pNL4-3 and either GFP [(−)Ctrl] or TIP47 expression vectors (pCMV-TIP47) at the indicated DNA concentrations. (A) Transfected cell lysates were probed with antibodies specific for tubulin and TIP47. (B) Cells were metabolically radiolabeled with [^{35}S]Cys; cell and virus lysates were immunoprecipitated with HIV-Ig. The relative ratios of virus-associated gp120 to p24(CA) were quantified by phosphorimager analysis (± SEM; $n = 3$). Using a paired *t* test, both samples overexpressing TIP47 were considered not significantly different from the negative control (two-tailed *P* values > 0.3) (C) Virus-containing supernatants were harvested from control and TIP47-overexpressing cells, normalized for RT activity, and used to infect the TZM-bl indicator cell line with four different virus inputs. Graphs show average levels of infectivity with a virus input of 50,000 RT cpm. Luciferase activity was measured 2 days postinfection (± SEM; $n = 3$).

RESULTS AND DISCUSSION

Recombinantly produced TIP47 is competent to bind its natural ligands. It has been demonstrated that preparations of TIP47, either recombinantly produced or endogenously purified, have low binding activity (21, 35, 36, 48). We therefore employed a surface plasmon resonance (SPR)-based interaction assay using two native ligands of TIP47, CD-M6PR and Rab9, to verify and quantify the activity of our full-length recombinant protein. Representative sensorgrams for these interactions are shown in Fig. 1. The apparent equilibrium dissociation constants (K_D) derived from fitting of the sensorgrams are in good agreement with values previously reported (35). These results demonstrate that our recombinant TIP47 protein is correctly folded and active (35, 36, 49–51).

The N terminus of TIP47 is required for its interaction with HIV-1 MA. To confirm the reported MA-TIP47 interaction (19) and define the domain of TIP47 required for binding, we performed SPR-based interaction analyses with purified MA protein and full-length or N-terminally truncated TIP47 protein (Fig. 2). We observed that HIV-1 MA binds well to the full-length TIP47 protein but does not bind the Δ1–186 TIP47 mutant. This implies that the N terminus of TIP47 is required for its interaction with HIV-1 MA. To place these results in the context of previous TIP47 binding studies, Hanna et al. showed that TIP47 residues 152 to 186 are required for Rab9 interaction (50) and Krise et al. demonstrated that the M6PR cytoplasmic domain interacts with the Δ1–186 TIP47 mutant (35).

To confirm these binding results by an independent approach,

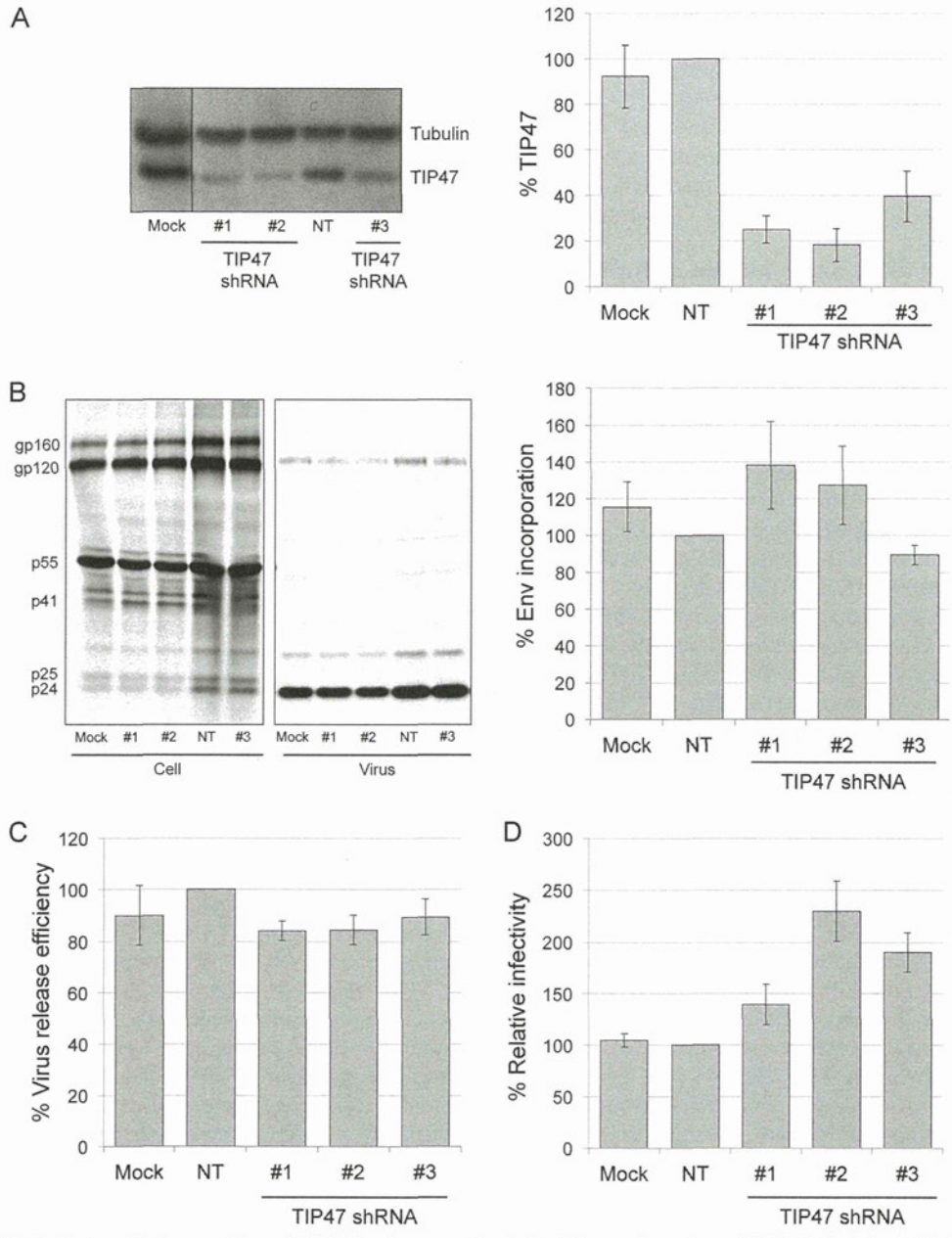

FIG 7 Depletion of TIP47 in Jurkat cells does not disrupt HIV-1 Env incorporation, infectivity, or virus release. (A) TIP47 depletion in Jurkat cells using shRNAs. TIP47 and tubulin were detected by Western blotting of puromycin-resistant Jurkat cells after transduction with TIP47-targeted shRNAs or nontargeting (NT) shRNA. Average protein levels relative to tubulin are shown. Error bars indicate SEM ($n = 3$). (B) HIV-1 Env incorporation efficiency in TIP47-depleted Jurkat cells. Cells were metabolically radiolabeled with [^{35}S]Cys; cell and virus lysates were immunoprecipitated with HIV-Ig (left panel). Average levels of Env incorporation are shown (right panel). Error bars indicate SEM ($n = 4$). Using a paired t test, none of the results were considered significantly different from the NT control results ($P > 0.05$). (C) HIV-1 release efficiency in TIP47-depleted Jurkat cells. Average virus release efficiency normalized to NT shRNA-transduced cells is shown. Error bars indicate SEM ($n = 4$). Using a paired t test, none of the results were considered significantly different from the NT control results ($P > 0.01$). (D) Infectivity of HIV-1 produced from TIP47-depleted Jurkat cells. Infectivity was detected by luciferase activity in infected TZM-bl cells, and results were averaged. Infectivity assays were performed with four different virus inputs, normalized for RT activity. Graphs show average levels of infectivity with a virus input of 25,000 RT cpm. Error bars indicate SEM ($n = 4$). Using a paired t test, the increases in infectivity were marginally significant relative to the controls ($P = 0.1$ for shRNA 2 compared to mock sample, and $P = 0.02$ for shRNA 2 compared to NT sample).

we performed ^{1}H-^{15}N HSQC experiments to probe for TIP47-MA binding. ^{1}H-^{15}N HSQC signals for the backbone amides of ^{15}N-labeled myristylated HIV-1 MA (myrMA) exhibited significant signal broadening upon titration with full-length TIP47 (Fig. 3A), which again indicates a direct interaction. The signals were nearly undetectable at TIP47/MA ratios above 1.0, consistent with tight binding and a dissociation equilibrium constant of less than ~100 μM. Similar results were obtained for the unmyristylated MA [myr(−)MA] protein, indicating that the myristyl group is not required for TIP47-MA binding (Fig. 3B). Consistent with the SPR data, titrations with TIP47 lacking the N-terminal oligomerization domain (Δ1–112 TIP47) did not affect the ^{1}H-^{15}N HSQC

spectra obtained for ^{15}N-labeled myrMA and myr(−)MA (Fig. 4A and B, respectively), which suggests no interaction. Similarly, titration of ^{15}N-labeled Δ1–112 TIP47 with myr(−)MA did not affect the ^{1}H-^{15}N HSQC spectrum of Δ1–112 TIP47 (Fig. 4C). These findings again indicate that the N-terminal domain of TIP47 is required for MA binding. However, neither the SPR nor the NMR approach excludes the possibility that oligomerization-dependent interactions between MA and the C-terminal domain of TIP47 may also exist.

Depletion of TIP47 in HeLa cells does not impair HIV-1 Env incorporation, virus release, or infectivity. To assess the putative role of TIP47 in Env incorporation, we depleted TIP47 in HeLa cells with a pool of four siRNAs. Nontargeting (NT) siRNA was used as a negative control. Cells were transfected with the pNL4-3 HIV-1 molecular clone and metabolically labeled with [^{35}S]Cys. Cell and virus lysates were immunoprecipitated with HIV-Ig. Levels of TIP47 were analyzed in parallel by quantitative Western blotting. Although TIP47 protein levels were significantly reduced (~90 to 95% depletion) (Fig. 5A), no significant decrease in Env (gp120) incorporation or virus release efficiency was observed (Fig. 5B). To evaluate the effect of TIP47 depletion on specific particle infectivity, viral supernatants were harvested from control and TIP47-depleted cells, normalized for RT activity, and used to infect the TZM-bl indicator cell line. No effect of TIP47 depletion on single-round infectivity was observed (Fig. 5C). These results indicate that depletion of 90 to 95% of TIP47 in HeLa cells does not affect Env incorporation, virus release efficiency, or HIV-1 infectivity.

Overexpression of TIP47 in HeLa cells does not enhance HIV-1 Env incorporation or virion infectivity. Lopez-Verges and coworkers (19) reported that overexpression of TIP47 in HeLa cells increases Env incorporation. To confirm this finding, HeLa cells were transfected with TIP47 or GFP (negative control) expression vectors and metabolically labeled with [^{35}S]Cys. Cell and virus lysates were immunoprecipitated with anti-HIV Ig. Despite markedly increased levels of TIP47 expression (Fig. 6A), no increase in HIV-1 Env incorporation was observed, as determined by the ratio of gp120/p24(CA) (Fig. 6B). We also measured the specific infectivity of virus released from TIP47-overexpressing cells in the TZM-bl single-cycle assay. No significant effect on particle infectivity was observed (Fig. 6C). These results demonstrate that TIP47 overexpression in HeLa cells does not enhance either Env incorporation or infectivity.

Depletion of TIP47 in Jurkat cells does not disrupt HIV-1 Env incorporation, virus release, infectivity, or replication. We previously demonstrated that the requirement for the gp41 CT in Env incorporation is cell type dependent; in HeLa cells, gp41 CT truncation had only a small effect on Env incorporation, whereas in most T-cell lines (e.g., Jurkat) the gp41 CT is required for Env incorporation and virus replication (16). These observations raised the possibility that TIP47 could play a cell type-dependent role in Env incorporation. We therefore depleted TIP47 in the Jurkat T-cell line by transducing with TIP47-specific shRNAs. Of five shRNAs tested, three yielded consistent knockdowns in the range of 60% for shRNA 3 and ~80% for shRNAs 1 and 2 (Fig. 7A); the others failed to produce reliable depletion (data not shown). To determine whether TIP47 depletion in Jurkat cells affects Env incorporation or virus release, TIP47-depleted cells were infected with VSV-G-pseudotyped HIV-1. Infected cells were then washed and labeled with [^{35}S]Cys for 4 h. Cell and virus lysates were immunoprecipitated, and Env incorporation and virus particle production were analyzed. We did not observe a significant decrease in Env (gp120) incorporation (Fig. 7B) or virus release efficiency (Fig. 7C). As a control, we compared levels of Env incorporation between wild-type (WT) (NL4-3) and a gp41 CT truncation mutant (NL4-3/CTdel-144) in Jurkat cells by applying the same VSV-G pseudotyping approach as the one used for TIP47-depleted Jurkat cells. As we reported previously (16), the CTdel-144 mutant displayed a 10-fold decrease in Env incorporation in Jurkat cells relative to the WT (data not shown). To determine the effect of TIP47 knockdown on HIV-1 infectivity, TZM-bl cells were infected with supernatants from TIP47-depleted, HIV-1-infected Jurkat cells. We did not observe a decrease in HIV-1 infectivity (Fig. 7D) but saw a small increase that was of marginal statistical significance (see legend to Fig. 7D). Finally, we tested whether TIP47 is required for the establishment of a spreading HIV-1 infection. TIP47-depleted Jurkat cells were transfected with pNL4-3, and virus replication was monitored by RT activity. We observed that HIV-1 replication in TIP47-depleted Jurkat cells peaked either on the same day as, or 2 days later than, replication in cells transduced with the nontargeting shRNA (Fig. 8). We observed a small amount of cytotoxicity in TIP47-depleted cells, likely accounting for the very minor delays in peak RT production in some cultures. TIP47 protein levels were analyzed close to the end of each replication assay; TIP47 knockdown efficiencies were calculated to be ~80% (data not shown). Because this level of TIP47 knockdown diminished after approximately 1 month, shRNA transductions were performed *de novo* for each experiment.

We note that Manrique and coworkers were able to detect an interaction between TIP47 and an HIV-1 gp41 CT-GST fusion but observed that TIP47 did not increase the binding of HIV-1 MA to the gp41 CT (52).

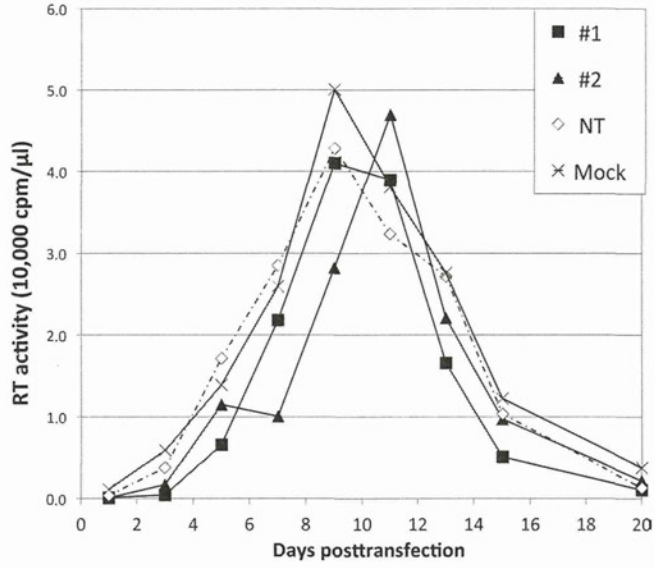

FIG 8 TIP47 depletion does not significantly affect HIV-1 replication in the Jurkat T-cell line. Jurkat cells transduced with shRNA 1 or 2 targeting TIP47 (#1 or #2) or nontargeting shRNA (NT) or Jurkat cells with no shRNA (mock) were transfected with the HIV-1 molecular clone pNL4-3 and passaged by dilution with fresh medium every 2 to 3 days. Culture supernatants were collected at each passage, and virus replication was monitored by RT activity.

In summary, the results of this study confirm the findings of Lopez-Verges et al. (19) indicating that HIV-1 MA binds to TIP47. However, our findings do not confirm a role for TIP47 in HIV-1 Env incorporation. It is possible that low levels of TIP47 could be sufficient to promote Env incorporation and that our depletions were not complete enough to induce an Env incorporation defect. However, the TIP47 depletion efficiencies observed in this study are similar to those achieved in studies that reported a requirement for TIP47 in Env incorporation, which was not quantified by Lopez-Verges et al. (19) but found to be in the 60 to 85% range by Bauby et al. (17). Further work will be required to delineate the physiological relevance to HIV-1 replication, if any, of the interaction between MA and TIP47.

ACKNOWLEDGMENTS

We thank members of the Freed laboratory for helpful discussion and critical review of the manuscript. The HIV-Ig and TZM-bl cells were obtained from the NIH AIDS Research and Reference Reagent Program. We thank C. Berlioz-Torrent for sharing reagents and for discussion of our results.

This research was supported by the Intramural Research Program of the Center for Cancer Research, National Cancer Institute, NIH, by the Intramural AIDS Targeted Antiviral Program, and by NIH/NIAID grants 1R03AI078790-01A1 (S.C.) and AI30917 (M.F.S.).

REFERENCES

1. **Checkley MA, Luttge BG, Freed EO.** 2011. HIV-1 envelope glycoprotein biosynthesis, trafficking, and incorporation. J. Mol. Biol. **410**:582–608.
2. **Balasubramaniam M, Freed EO.** 2011. New insights into HIV assembly and trafficking. Physiology **26**:236–251.
3. **Sundquist WI, Krausslich HG.** 2012. HIV-1 assembly, budding, and maturation. Cold Spring Harb. Perspect. Med. **2**:a006924. doi:10.1101/cshperspect.a006924.
4. **Johnson MC.** 2011. Mechanisms for Env glycoprotein acquisition by retroviruses. AIDS Res. Hum. Retroviruses **27**:239–247.
5. **Dorfman T, Mammano F, Haseltine WA, Gottlinger HG.** 1994. Role of the matrix protein in the virion association of the human immunodeficiency virus type 1 envelope glycoprotein. J. Virol. **68**:1689–1696.
6. **Freed EO, Martin MA.** 1996. Domains of the human immunodeficiency virus type 1 matrix and gp41 cytoplasmic tail required for envelope incorporation into virions. J. Virol. **70**:341–351.
7. **Freed EO, Martin MA.** 1995. Virion incorporation of envelope glycoproteins with long but not short cytoplasmic tails is blocked by specific, single amino acid substitutions in the human immunodeficiency virus type 1 matrix. J. Virol. **69**:1984–1989.
8. **Mammano F, Kondo E, Sodroski J, Bukovsky A, Gottlinger HG.** 1995. Rescue of human immunodeficiency virus type 1 matrix protein mutants by envelope glycoproteins with short cytoplasmic domains. J. Virol. **69**:3824–3830.
9. **Murakami T, Freed EO.** 2000. Genetic evidence for an interaction between human immunodeficiency virus type 1 matrix and alpha-helix 2 of the gp41 cytoplasmic tail. J. Virol. **74**:3548–3554.
10. **Reil H, Bukovsky AA, Gelderblom HR, Gottlinger HG.** 1998. Efficient HIV-1 replication can occur in the absence of the viral matrix protein. EMBO J. **17**:2699–2708.
11. **Yu X, Yuan X, Matsuda Z, Lee TH, Essex M.** 1992. The matrix protein of human immunodeficiency virus type 1 is required for incorporation of viral envelope protein into mature virions. J. Virol. **66**:4966–4971.
12. **Cronin J, Zhang XY, Reiser J.** 2005. Altering the tropism of lentiviral vectors through pseudotyping. Curr. Gene Ther. **5**:387–398.
13. **Page KA, Landau NR, Littman DR.** 1990. Construction and use of a human immunodeficiency virus vector for analysis of virus infectivity. J. Virol. **64**:5270–5276.
14. **Waheed AA, Freed EO.** 2010. The role of lipids in retrovirus replication. Viruses **2**:1146–1180.
15. **Akari H, Fukumori T, Adachi A.** 2000. Cell-dependent requirement of human immunodeficiency virus type 1 gp41 cytoplasmic tail for Env incorporation into virions. J. Virol. **74**:4891–4893.
16. **Murakami T, Freed EO.** 2000. The long cytoplasmic tail of gp41 is required in a cell type-dependent manner for HIV-1 envelope glycoprotein incorporation into virions. Proc. Natl. Acad. Sci. U. S. A. **97**:343–348.
17. **Bauby H, Lopez-Verges S, Hoeffel G, Delcroix-Genete D, Janvier K, Mammano F, Hosmalin A, Berlioz-Torrent C.** 2010. TIP47 is required for the production of infectious HIV-1 particles from primary macrophages. Traffic **11**:455–467.
18. **Blot G, Janvier K, Le Panse S, Benarous R, Berlioz-Torrent C.** 2003. Targeting of the human immunodeficiency virus type 1 envelope to the trans-Golgi network through binding to TIP47 is required for env incorporation into virions and infectivity. J. Virol. **77**:6931–6945.
19. **Lopez-Verges S, Camus G, Blot G, Beauvoir R, Benarous R, Berlioz-Torrent C.** 2006. Tail-interacting protein TIP47 is a connector between Gag and Env and is required for Env incorporation into HIV-1 virions. Proc. Natl. Acad. Sci. U. S. A. **103**:14947–14952.
20. **Hickenbottom SJ, Kimmel AR, Londos C, Hurley JH.** 2004. Structure of a lipid droplet protein; the PAT family member TIP47. Structure **12**:1199–1207.
21. **Sincock PM, Ganley IG, Krise JP, Diederichs S, Sivars U, O'Connor B, Ding L, Pfeffer SR.** 2003. Self-assembly is important for TIP47 function in mannose 6-phosphate receptor transport. Traffic **4**:18–25.
22. **Diaz E, Pfeffer SR.** 1998. TIP47: a cargo selection device for mannose 6-phosphate receptor trafficking. Cell **93**:433–443.
23. **Lombardi D, Soldati T, Riederer MA, Goda Y, Zerial M, Pfeffer SR.** 1993. Rab9 functions in transport between late endosomes and the trans Golgi network. EMBO J. **12**:677–682.
24. **Riederer MA, Soldati T, Shapiro AD, Lin J, Pfeffer SR.** 1994. Lysosome biogenesis requires Rab9 function and receptor recycling from endosomes to the trans-Golgi network. J. Cell Biol. **125**:573–582.
25. **Bulankina AV, Deggerich A, Wenzel D, Mutenda K, Wittmann JG, Rudolph MG, Burger KN, Honing S.** 2009. TIP47 functions in the biogenesis of lipid droplets. J. Cell Biol. **185**:641–655.
26. **Bickel PE, Tansey JT, Welte MA.** 2009. PAT proteins, an ancient family of lipid droplet proteins that regulate cellular lipid stores. Biochim. Biophys. Acta **1791**:419–440.
27. **Wolins NE, Rubin B, Brasaemle DL.** 2001. TIP47 associates with lipid droplets. J. Biol. Chem. **276**:5101–5108.
28. **Hynson RM, Jeffries CM, Trewhella J, Cocklin S.** 2012. Solution structure studies of monomeric human TIP47/perilipin-3 reveal a highly extended conformation. Proteins **80**:2046–2055.
29. **Massiah MA, Starich MR, Paschall C, Summers MF, Christensen AM, Sundquist WI.** 1994. Three-dimensional structure of the human immunodeficiency virus type 1 matrix protein. J. Mol. Biol. **244**:198–223.
30. **Tang C, Loeliger E, Luncsford P, Kinde I, Beckett D, Summers MF.** 2004. Entropic switch regulates myristate exposure in the HIV-1 matrix protein. Proc. Natl. Acad. Sci. U. S. A. **101**:517–522.
31. **Delaglio F, Grzesiek S, Vuister GW, Zhu G, Pfeifer J, Bax A.** 1995. NMRPipe: a multidimensional spectral processing system based on UNIX pipes. J. Biomol. NMR **6**:277–293.
32. **Johnson BA.** 2004. Using NMRView to visualize and analyze the NMR spectra of macromolecules. Methods Mol. Biol. **278**:313–352.
33. **Weeks SD, Drinker M, Loll PJ.** 2007. Ligation independent cloning vectors for expression of SUMO fusions. Protein Expr. Purif. **53**:40–50.
34. **Studier FW.** 2005. Protein production by auto-induction in high density shaking cultures. Protein Expr. Purif. **41**:207–234.
35. **Krise JP, Sincock PM, Orsel JG, Pfeffer SR.** 2000. Quantitative analysis of TIP47-receptor cytoplasmic domain interactions: implications for endosome-to-trans Golgi network trafficking. J. Biol. Chem. **275**:25188–25193.
36. **Orsel JG, Sincock PM, Krise JP, Pfeffer SR.** 2000. Recognition of the 300-kDa mannose 6-phosphate receptor cytoplasmic domain by 47-kDa tail-interacting protein. Proc. Natl. Acad. Sci. U. S. A. **97**:9047–9051.
37. **Chen L, DiGiammarino E, Zhou XE, Wang Y, Toh D, Hodge TW, Meehan EJ.** 2004. High resolution crystal structure of human Rab9 GTPase: a novel antiviral drug target. J. Biol. Chem. **279**:40204–40208.
38. **Adachi A, Gendelman HE, Koenig S, Folks T, Willey R, Rabson A, Martin MA.** 1986. Production of acquired immunodeficiency syndrome-associated retrovirus in human and nonhuman cells transfected with an infectious molecular clone. J. Virol. **59**:284–291.
39. **Freed EO, Englund G, Martin MA.** 1995. Role of the basic domain of human immunodeficiency virus type 1 matrix in macrophage infection. J. Virol. **69**:3949–3954.

40. **Freed EO, Martin MA.** 1994. HIV-1 infection of non-dividing cells. Nature **369**:107–108.
41. **Freed EO, Martin MA.** 1994. Evidence for a functional interaction between the V1/V2 and C4 domains of human immunodeficiency virus type 1 envelope glycoprotein gp120. J. Virol. **68**:2503–2512.
42. **Willey RL, Bonifacino JS, Potts BJ, Martin MA, Klausner RD.** 1988. Biosynthesis, cleavage, and degradation of the human immunodeficiency virus 1 envelope glycoprotein gp160. Proc. Natl. Acad. Sci. U. S. A. **85**: 9580–9584.
43. **Naldini L, Blomer U, Gallay P, Ory D, Mulligan R, Gage FH, Verma IM, Trono D.** 1996. In vivo gene delivery and stable transduction of nondividing cells by a lentiviral vector. Science **272**:263–267.
44. **Yee JK, Miyanohara A, LaPorte P, Bouic K, Burns JC, Friedmann T.** 1994. A general method for the generation of high-titer, pantropic retroviral vectors: highly efficient infection of primary hepatocytes. Proc. Natl. Acad. Sci. U. S. A. **91**:9564–9568.
45. **Checkley MA, Luttge BG, Soheilian F, Nagashima K, Freed EO.** 2010. The capsid-spacer peptide 1 Gag processing intermediate is a dominant-negative inhibitor of HIV-1 maturation. Virology **400**:137–144.
46. **Luttge BG, Shehu-Xhilaga M, Demirov DG, Adamson CS, Soheilian F, Nagashima K, Stephen AG, Fisher RJ, Freed EO.** 2008. Molecular characterization of feline immunodeficiency virus budding. J. Virol. **82**: 2106–2119.
47. **Kiernan RE, Ono A, Englund G, Freed EO.** 1998. Role of matrix in an early postentry step in the human immunodeficiency virus type 1 life cycle. J. Virol. **72**:4116–4126.
48. **Burguete AS, Sivars U, Pfeffer S.** 2005. Purification and analysis of TIP47 function in Rab9-dependent mannose 6-phosphate receptor trafficking. Methods Enzymol. **403**:357–366.
49. **Ganley IG, Carroll K, Bittova L, Pfeffer S.** 2004. Rab9 GTPase regulates late endosome size and requires effector interaction for its stability. Mol. Biol. Cell **15**:5420–5430.
50. **Hanna J, Carroll K, Pfeffer SR.** 2002. Identification of residues in TIP47 essential for Rab9 binding. Proc. Natl. Acad. Sci. U. S. A. **99**:7450–7454.
51. **Zentner IJ, Cocklin. S.** Analysis of protein-protein interactions using surface plasmon resonance biosensing, in press. Research Signpost Publishing, Kerala, India.
52. **Manrique JM, Affranchino JL, Gonzalez SA.** 2008. In vitro binding of simian immunodeficiency virus matrix protein to the cytoplasmic domain of the envelope glycoprotein. Virology **374**:273–279.

JVI
Journals.ASM.org

Cyclophilin A-Dependent Restriction to Capsid N121K Mutant Human Immunodeficiency Virus Type 1 in a Broad Range of Cell Lines

Taichiro Takemura, Miyako Kawamata, Miho Urabe, Tsutomu Murakami

AIDS Research Center, National Institute of Infectious Diseases, Shinjuku-ku, Tokyo, Japan

Human immunodeficiency virus type 1 (HIV-1) infection of most human cells is dependent on cyclophilin A (CypA); however, the opposite phenomenon, known as CypA-dependent inhibition, is also observed in the combination of some capsid (CA) mutations and cell lines. Here, we identified a CA N121K mutant whose infection of 293T, Jurkat, and HeLa cells was impaired by CypA. The N121K mutant could be a useful tool for analyzing the mechanisms underlying CypA-dependent restriction.

The host cellular protein cyclophilin A (CypA) binds to the proline-rich loop in the N-terminal region of the human immunodeficiency virus type 1 (HIV-1) capsid (CA) protein (1, 2). Inhibition of the CA-CypA interaction by using competitive chemicals such as cyclosporine (CsA), introduction of mutations into the CypA-binding loop within CA, or RNA interference (RNAi)-mediated knockdown of endogenous CypA in target cells leads to reduced HIV-1 infectivity (3, 4). An initial model assumed that the incorporation of CypA into the virions facilitates uncoating of the HIV-1 core. However, recent studies show that the CA-CypA interaction in target cells, rather than that of virus-incorporated CypA, is important for HIV-1 infection (5, 6). CypA catalyzes the *cis-trans* isomerization of proline peptide bonds, leading to conformational changes in CA and, in turn, the core structure. Although the CA-CypA interaction has been well characterized *in vitro*, the precise role played by CypA during HIV-1 replication is still unclear (3, 4). Recent reports indicate that the CA-CypA interaction is involved not only in uncoating but also in nuclear import and integration (7, 8).

HIV-1 infection of most human cells is dependent on CypA; however, the opposite phenomenon, known as CypA-dependent inhibition, is observed for some CA mutant viruses. A previous study showed that the passage of wild-type (WT) HIV-1 in HeLa-CD4 cells (when CypA was inhibited by CsA) resulted in the generation of two CA escape mutants, A92E and G94D (9). These mutations tolerate the inhibition of CA-CypA interaction, but their replication in HeLa and H9 cells (although not in other cell lines such as 293T and Jurkat cells) becomes dependent on CsA (6, 10). Several CA mutants, such as R132K and T54A, showed similar CsA-dependent phenotypes in a target cell-contingent manner (11–13). These results imply the bidirectional function of CypA during HIV-1 replication. To better understand the function of CypA during HIV-1 replication, the viral regions that modulate CypA dependence must be identified. To this end, we tried to isolate HIV-1 mutants that can replicate in Jurkat cells in the absence of CypA. The newly isolated CA mutant N121K was generated by serial passage of a CypA-nonbinding HIV-1 mutant (NL4-3.P90A.A92E) in Jurkat cells (14). In this paper, we report that N121K infection is inhibited in a CypA-dependent manner not only in HeLa and H9 cells but also in 293T and Jurkat cells.

We attempted to isolate HIV-1 mutants that replicate in Jurkat cells in the absence of CypA; HIV-1 infection of Jurkat cells is CypA dependent. Jurkat cells were infected with either WT virus or a CypA-nonbinding mutant, NL4-3.P90A.A92E, in the presence or absence of 1 μM cyclosporine (CsA) as follows: culture I, NL4-3 without CsA; culture II, NL4-3 plus 1 μM CsA; culture III, NL4-3.P90A.A92E without CsA; and culture IV, NL4-3.P90A.A92E plus 1 μM CsA. After repeated passage (47 times), we succeeded in obtaining replication-competent viruses under all culture conditions. Sequence analysis of the entire *gag* region identified a virus from culture II that harbored a mutation in MA (V34I). The CA N121K and CA R132K mutants arose from cultures III and IV, respectively. The mutation in MA overlapped with a mutation reported to increase viral fitness in T-cell cultures (15). Therefore, we studied two CA mutant viruses in detail. Since the R132K substitution identified in the virus from culture IV had also been identified previously (11, 16), we focused on the N121K mutant (which harbored a mutation in the loop between helix 6 and helix 7), which arose from culture III (Jurkat cells infected with NL4-3.P90A.A92E in the absence of CsA).

We constructed an N121K substitution virus on a WT (NL4-3 or NL4-3-luc) and the CypA-nonbinding mutant (NL4-3.P90A.A92E or NL4-3.P90A.A92E-luc) backbone. Viral replication was then examined in Jurkat and H9 cells, and infection efficiency was examined in Jurkat, 293T, and HeLa cells. Figure 1A to D shows the replication kinetics of the WT and CA mutant viruses in Jurkat and H9 cells in the presence or absence of 1 μM CsA. The triple mutant virus (N121K.P90A.A92E) replicated as efficiently as did the WT virus in the presence or absence of CsA in both cell lines. However, the replication of the N121K single mutant virus in both Jurkat and H9 cells increased in the presence of CsA (Fig. 1B and D). Similar results were observed in the single-round infection experiments (Fig. 1E to G). Infection by the N121K.P90A.A92E mutant was not impaired in any of the cell lines, in either the presence or the absence of CsA. However, the

Received 30 May 2012 Accepted 7 January 2013
Published ahead of print 16 January 2013
Address correspondence to Taichiro Takemura, taichiro@nih.go.jp, or Tsutomu Murakami, tmura@nih.go.jp.

doi:10.1128/JVI.01319-12

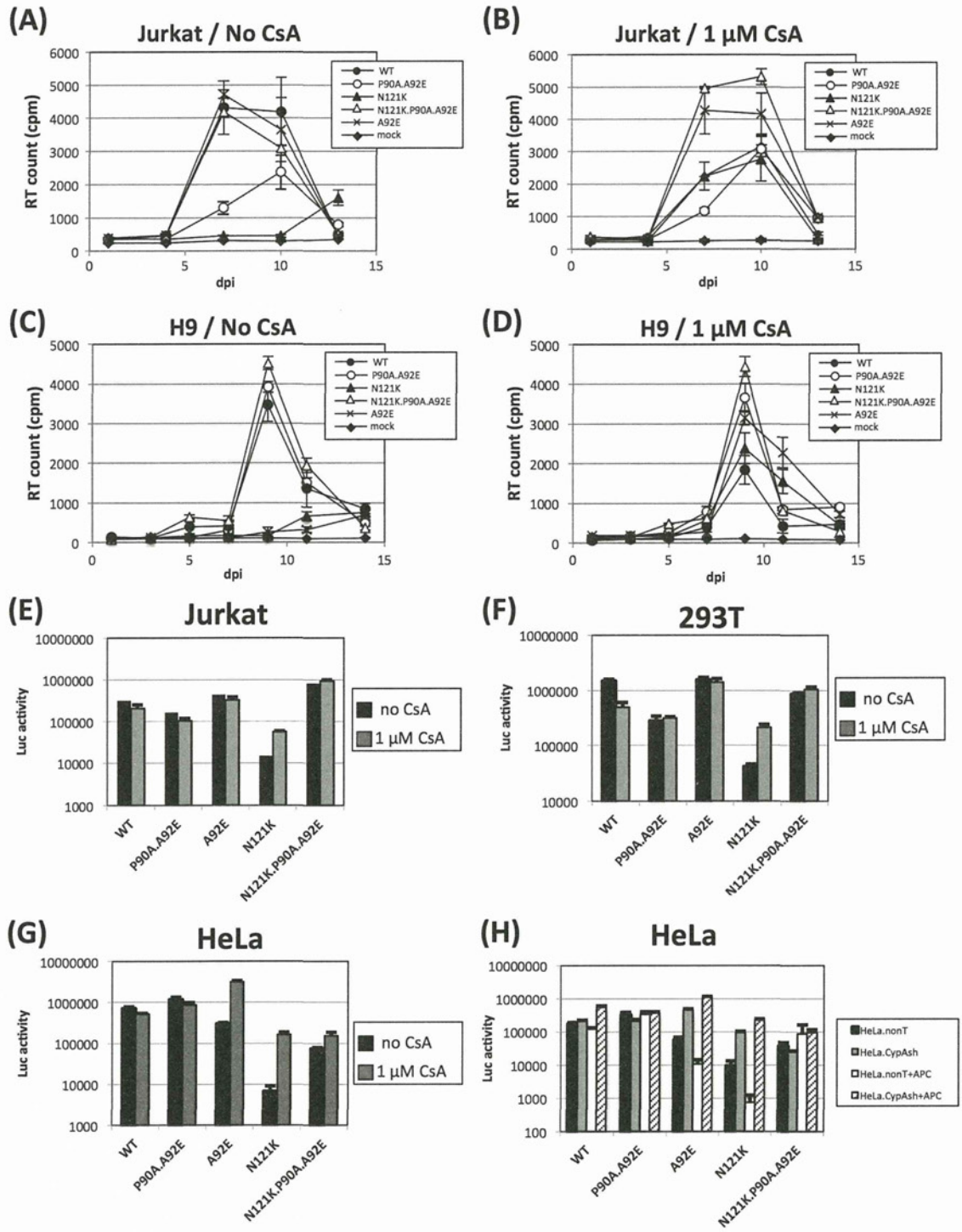

FIG 1 Inhibition of the CA-CypA interaction rescues the infectivity of N121K HIV-1. (A to D) Jurkat (A and B) or H9 (C and D) cells were infected with 1 ng of p24 of wild-type (WT) or CA mutant (P90A.A92E, A92E, N121K, and N121K.P90A.A92E) HIV-1 in the presence or absence of 1 μM CsA. Virus replication was determined by enzyme-linked immunosorbent assay of p24 in the culture supernatant. (E to G) Jurkat (E), 293T (F), or HeLa (G) cells were infected (in the presence or absence of CsA) with vesicular stomatitis virus G protein-pseudotyped WT or CA mutant viruses carrying the luciferase gene. After 48 h, cellular luciferase activity was determined using the Steady-Glo luciferase assay system (Promega). (H) HeLa cells were transduced with vectors expressing a nontarget (nonT) or CypA-targeted short hairpin RNA (CypAsh) in the absence or presence of 10 μg/ml of aphidicolin (APC; Sigma-Aldrich) and then infected with the pseudotyped WT or CA mutant viruses. Error bars represent the standard deviations (from parallel cultures performed in triplicate). The results are representative of at least three independent experiments.

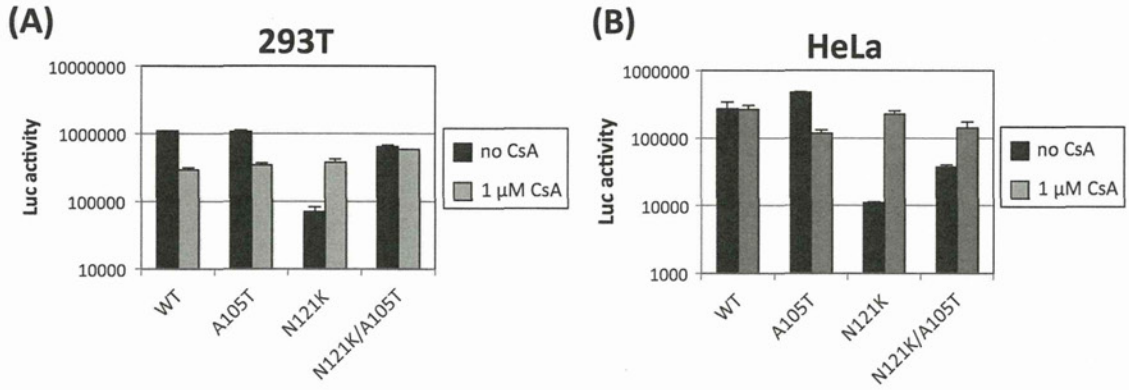

FIG 2 Rescue of N121K HIV-1 infection by the CA A105T mutation. Single-cycle infectivity was determined by infection with the vesicular stomatitis virus G protein-pseudotyped CA mutant virus carrying the luciferase gene. A total of 5×10^4 293T (A) or HeLa (B) cells were inoculated with 1 ng of p24 from each virus. After 48 h, the luciferase activity was measured. Error bars represent the standard deviations (for parallel cultures performed in triplicate). The results are representative of at least three independent experiments.

infection of Jurkat, 293T, and HeLa cells by N121K increased in the presence of 1 μM CsA.

Previous studies show that CypA-dependent inhibition of infection by some CA mutants is greater in nondividing cells (16, 17). Therefore, to investigate whether the mechanism underlying the CypA-dependent inhibition of infection by N121K mutants is similar to that observed for other CA mutants such as A92E, we tested whether cell growth arrest of CypA- or nontarget short hairpin RNA (shRNA)-transduced HeLa cells further inhibited infection by N121K. CypA knockdown by shRNA restored the infection efficiency of the N121K mutant (Fig. 1H), suggesting that N121K is inhibited by CypA in the cytoplasm of the target cells as previously observed for other CsA-dependent mutant viruses (5, 18). Aphidicolin-induced growth arrest markedly increased the level of N121K inhibition in HeLa cells (as was observed in A92E mutants) (16, 17).

The A105T mutation is suppressive in CsA-dependent CA mutants, such as A92E (12). Therefore, we next asked whether the A105T mutation suppressed the inhibition of N121K infectivity in 293T and HeLa cells. The infectivity of a dual mutant (N121K.A105T) virus was approximately 10-fold higher than that of a single mutant N121K virus in both 293T and HeLa cells. The A105T mutation fully restored the infection efficiency of the N121K mutant virus in 293T cells (Fig. 2A). In contrast, the A105T-mediated rescue of infection efficiency in HeLa cells was only moderate, and it was increased by the addition of CsA (Fig. 2B). Interestingly, the infection efficiency of the single A105T mutant decreased in both HeLa cells and 293T cells in the presence of CsA. Yang and Aiken suggested two possible explanations for why the A105T mutation may compensate for the structural changes caused by CypA or block the potent inhibitory factor activated by CypA-dependent manner (12).

We next determined which N121K replication step(s) is regulated by cellular CypA by measuring the synthesis of new reverse transcription (RT) products, or the production of two-long-terminal-repeat (2-LTR) circular DNA products, by quantitative real-time PCR (19) in the presence or absence of 1 μM CsA. Viral infectivity was also measured in parallel (Fig. 3A). There was no clear difference between the early and late N121K RT products in the presence or absence of CsA (Fig. 3B and C). However, the addition of CsA increased the amount of N121K 2-LTR circular DNA products (Fig. 3D). These results indicate that the replication of N121K is impaired at the nuclear transport stage. Although it is thought that the inhibition of these viruses occurs at either the RT, nuclear import, or integration stages, the replication step impaired by CypA (with regard to the A92E and G94D mutant viruses) is still controversial (12, 16, 17, 20). Our quantitative PCR data show that the inhibition of N121K replication occurs at the nuclear import stage, supporting previous data showing that the CA-CypA interaction is involved in a series of viral replication steps at the nuclear import stage (8, 17).

Next, we conducted infection experiments by titrating the dose of CsA and examining the effects on the infectivity of WT, A92E, and N121K viruses. 293T or HeLa cells were incubated with 0.5 ng of virus p24 in the presence of increasing concentrations of CsA. Along with the increase of the CsA concentration, the infectivity of the WT virus gradually decreased to approximately one-fifth of that of the virus in the control infection without CsA in 293T cells (Fig. 4A). The infectivity of the A92E virus was not affected by the CsA concentration in 293T cells. In contrast, the infectivity of the N121K virus gradually increased with increasing CsA concentration (up to 0.15 μM CsA). The infection efficiencies of N121K and the WT virus were comparable at CsA concentrations above 1.25 μM. In HeLa cells, the titration curve for the N121K virus was similar to that of the A92E virus; however, the infectivity of N121K was less than that of A92E at most CsA concentrations tested (Fig. 4B). The dual mutant virus (N121K.A92E) also showed increased infectivity in line with the increasing CsA concentration, although the infectivity was about 10-fold less than that of N121K in 293T cells and that of A92E and N121K in HeLa cells. This suggests that CypA-dependent restriction of the N121K.A92E dual mutant is increased in both cell types. Although the underlying mechanisms are still unclear, these data suggest that the CypA-dependent restriction factor(s) is expressed at different levels in 293T and HeLa cells. If the sensitivity of N121K to this hypothetical factor is higher than that of A92E, this may account for the different infectivities of A92E in 293T and HeLa cells. N121K might be very sensitive to this factor, and the A92E.N121K mutant is even more sensitive because A92E is potently restricted by the as-yet-unknown factor. This hypothesis can explain the different levels of N121K toleration shown by the introduction of an additional A105T mutation shown in Fig. 2.

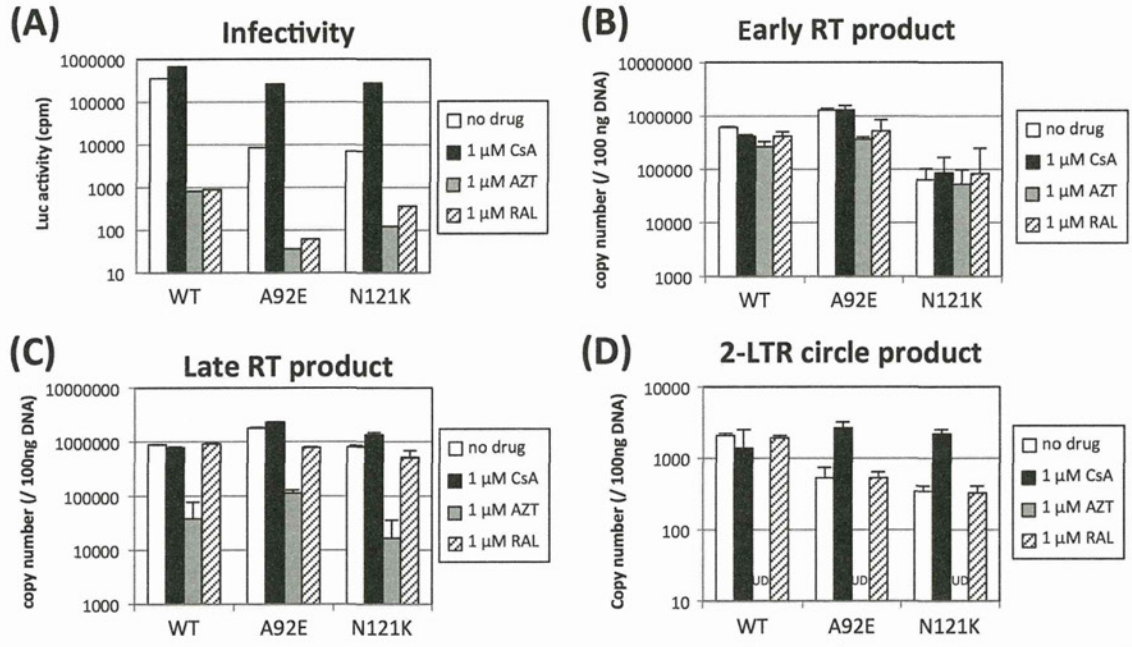

FIG 3 The replication defect observed in N121K virus occurs at the nuclear import stage. HeLa cells (2×10^5) were infected with 4 ng of p24 from vesicular stomatitis virus G protein-pseudotyped WT, A92E, or N121K virus (harboring the luciferase gene). The infection was performed under the following conditions: no drug, 1 μM CsA, 1 μM azidothymidine (AZT; Sigma-Aldrich), and 1 μM raltegravir (RAL). (A) Virus infectivity was determined by measuring the luciferase activity 2 days after infection. Total DNA was extracted 24 h (B and C) or 36 h (D) after infection, and 200 ng of the DNA was subjected to quantitative PCR (19). The error bars represent the standard deviations from duplicate assays performed in a single experiment. The results are representative of two independent experiments. UD, undetectable.

In this report, we infected 293T, Jurkat, and HeLa cells with a CA mutant virus, N121K, which has a CsA-dependent phenotype. Although a similar CsA-dependent mutant virus, such as A92E, was previously identified, the CsA dependence was observed only in high-CypA-expressing cells, such as HeLa and H9 (9, 11, 12, 21). Two hypotheses have been proposed to explain CsA-dependent infection by CA mutants. The first is that high levels of cellular CypA alter the stability and uncoating of the mutant viral core; the second is that a potent, as-yet-unknown HIV-1-inhibitory factor(s) interrupts the proper timing of uncoating or disrupts nuclear import or integration (5, 12, 18, 20). In the present study, N121K replication was disrupted after the RT step and the magnitude of this inhibition varied in a cell-type-dependent manner. Inhibition of N121K virus infection appears to be stronger in HeLa cells than in 293T cells, and this can be explained by the potent as-yet-unknown restrictive factor differentially expressed in 293T and HeLa cells. Further work is needed to validate this model. The N121K mutation is located in the loop between helices 6 and 7. Two different groups reported that human TRIM5α inhibits N-tropic murine leukemia virus (N-MLV) infection in human cells by recognizing a comparable region within the viral CA (in the loop between helix 6 and helix 7) (22, 23). Considering the conformational homology between N-MLV and HIV-1, this region might be accessible to human TRIM5α. We knocked down

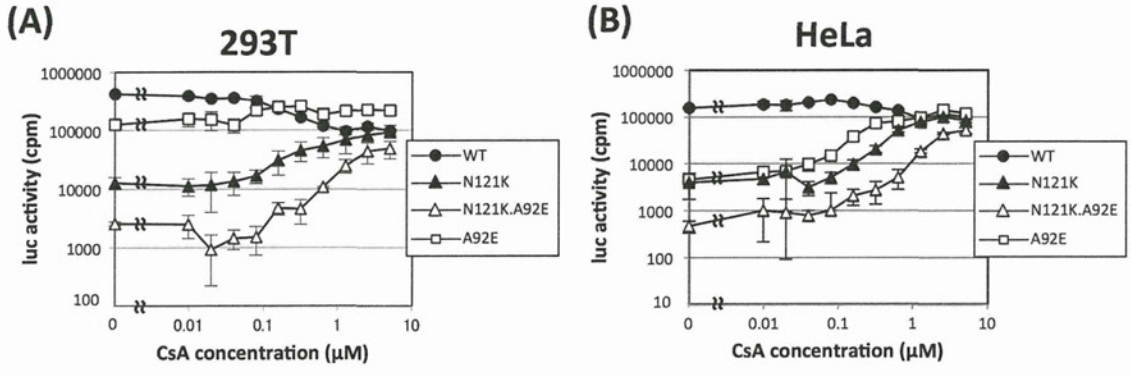

FIG 4 Effects of titrating CsA on the infectivity of WT, A92E, N121K, and N121K.A92E HIV-1. In the presence of different concentrations of CsA, 4×10^4 293T cells (A) or HeLa cells (B) were infected with 0.5 ng of p24 from vesicular stomatitis virus G protein-pseudotyped HIV-1 carrying the luciferase gene as a marker. Cellular luciferase activity was measured after 48 h. The error bars represent the standard deviations from parallel cultures performed in triplicate. The results are representative of two independent experiments.